

Title:

**A femto-molar range suicide germination stimulant for the parasitic plant
*Striga hermonthica***

Authors:

Daisuke Uraguchi^{1*}, Keiko Kuwata², Yuh Hijikata^{2,3}, Rie Yamaguchi², Hanae Imaizumi²,
Sathiyarayanan AM², Christin Rakers^{3†}, Narumi Mori⁴, Kohki Akiyama⁴, Stephan
Irle^{2,3‡}, Peter McCourt⁵, Toshinori Kinoshita^{2,3}, Takashi Ooi^{1,2,6*}, Yuichiro Tsuchiya^{2*}

Affiliations:

¹Graduate School of Engineering, Nagoya University, Furo-cho, Chikusa-ku, Nagoya 464-8603, Japan.

²Institute of Transformative Bio-Molecules (WPI-ITbM), Nagoya University, Furo-cho, Chikusa-ku, Nagoya 464-8601, Japan.

³Graduate School of Science, Nagoya University, Furo-cho, Chikusa-ku, Nagoya 464-8602, Japan.

⁴Graduate School of Life and Environmental Sciences, Osaka Prefecture University, 1-1 Gakuen-cho, Naka-ku, Sakai, Osaka 599-8531, Japan

⁵Department of Cell & Systems Biology, University of Toronto, 25 Willcocks Street, Toronto M5S 3B2, Canada.

⁶CREST, Japan Science and Technology Agency (JST), Nagoya University, Nagoya 464-8601, Japan.

[†]Present address: Graduate School of Pharmaceutical Sciences, Kyoto University, 46-29 Yoshida-Shimo-Adachi-cho, Sakyo-ku, Kyoto 606-8501, Japan.

[‡]Present address: Computational Sciences and Engineering Division & Chemical Sciences Division, Oak Ridge National Laboratory, Oak Ridge, Tennessee 37831, USA.

*Correspondence to:

Daisuke Uraguchi: uraguchi@chembio.nagoya-u.ac.jp

Takashi Ooi: tooi@chembio.nagoya-u.ac.jp

Yuichiro Tsuchiya: yuichiro@itbm.nagoya-u.ac.jp

Abstract:

The parasitic plant *Striga hermonthica* has been causing devastating damages to the crop production in Africa. As *Striga* requires host-generated strigolactones to germinate, the identification of selective and potent strigolactone agonists could help control these noxious weeds. Herein, we developed a selective agonist, sphynolactone-7, a hybrid molecule originated from chemical screening, containing two functional modules derived from a synthetic scaffold and a core component of strigolactones. Cooperative action of these modules in the activation of a high affinity strigolactone receptor ShHTL7 allows sphynolactone-7 to provoke *Striga* germination with potency in the femtomolar range. We demonstrate that sphynolactone-7 is effective for reducing *Striga* parasitism without impinging on host strigolactone-related processes.

One Sentence Summary:

A hypersensitive hybrid molecule agonist for a key strigolactone receptor in the parasitic weed *Striga hermonthica*.

Main text:

Striga hermonthica (*Striga*) parasitizes crops widely across various parts of sub-Saharan Africa, causing loss in crop yields that result in economic pressure on millions of smallholder farmers and lead to annual losses of billions of dollars (1). Protecting crops from the numerous tiny *Striga* seeds buried in the soil requires integration of various approaches to suppress infestation (1). A group of host-generated small molecule hormones, called strigolactones (SLs), provoke germination of *Striga* seeds. Because *Striga* is an obligate parasite, germination in the absence of a host is lethal and this has prompted researchers to develop SL agonists as inducers of suicidal germination to purge the soil of viable *Striga* seeds (2). This approach requires the development of potent and accessible compounds that only act on *Striga* and do not impede normal crop development. For example, SLs are also plant chemical cues that attract root symbiotic arbuscular mycorrhizal fungi (AM fungi) that supply host plants with nutrients (3, 4). Herein, we report the development of a *Striga*-selective SL agonist acting in the femtomolar range.

SLs are a group of plant-derived molecules whose structures consist of butenolide rings (D-ring), which are connected to cyclic moieties, usually three-ring systems (ABC-ring), through an enol-ether bridge (Fig. 1A). In vascular plants, SLs are plant hormones that optimize plant body architectures through the *DWARF14* (*D14*) family of α/β hydrolase-fold receptors (5). D14 defines a non-canonical receptor because it initiates signal transduction by utilizing enzymatic activity. Upon binding, SLs undergo cleavage of the enol-ether bridge through hydrolysis to leave the D-ring as a covalently-linked intermediate

1 molecule (CLIM) at the catalytic histidine residue in the receptor (6-8). Previous studies
2 suggest that the ABC-portion of the SL is released from the D14 pocket, and the receptor–
3 CLIM complex alters D14 conformation to recruit downstream negative regulators such as
4 the SCF^{MAX2} protein (7). In *Striga*, it is thought that SLs trigger seed germination through
5 11 members of an independently diverged α/β hydrolase-fold receptors called *Striga*
6 *HYPOSENSITIVE TO LIGHT/KARRIKIN INSENSITIVE2* (*ShHTL/KAI2* herein called
7 *ShHTLs*) (9-11). The hydrolytic activity of ShHTLs was exploited in the development of
8 fluorogenic SL probes to uncover an ethylene-mediated amplification of a wave-like
9 pattern of SL perception initiated during *Striga* germination (10). Moreover, *in vitro*
10 binding suggests that the divergence of ligand preferences in ShHTLs is beneficial for
11 *Striga* seeds to detect the blend of SLs exuding from preferred host species (10). Among
12 these ShHTL isoforms, we have focused on ShHTL7, as this receptor is sensitive to
13 picomolar levels of SLs when heterologously expressed in *Arabidopsis*, and its large
14 binding pocket ensures a response to structurally diverse molecules (11, 12). These
15 characteristics make ShHTL7 a suitable target for the development of agonists for
16 stimulating *Striga* germination.

17
18 Chemical analysis on SLs over the past 40 years suggests that the structure of the D-ring is
19 essential to SL activity (2, 3). By contrast, structural flexibility in the ABC-portion has led
20 to the development of various synthetic SLs or SL-mimics including GR24 or simplified
21 phenol-D-ring derivatives called debranones (2, 13). However, the structural element of the
22 ABC-portion that contributes to both potency and specificity to *Striga* remains elusive. To

1 further explore the chemical characteristics that define species selectivity towards *Striga*,
2 we performed a small molecule screen for compounds that germinate *Striga* seeds (harvests
3 from sorghum fields in Sudan). The screening of 12,000 synthetic molecules was followed
4 by additional synthesis of 60 analogs of hit compounds that were found from the initial
5 screening. Based on median inhibitory concentration (IC₅₀) using the fluorogenic SL-mimic
6 Yoshimulactone Green (YLG) resulted in the identification of *N*-arylsulfonylpiperazine as a
7 molecular scaffold that selectively bound to ShHTL7 (Fig. 1A-B, fig. S1, and table S1). A
8 representative molecule, SAM690, which contains the arylsulfonylpiperazine moiety,
9 exhibited potency towards *Striga* germination at the μ M level. The mode of action of
10 SAM690 was similar to (+)-GR24, in that germination activity was suppressed by
11 inhibition of ethylene production (Fig. 1C). However, unlike (+)-GR24, SAM690 was not
12 hydrolyzed by ShHTL7 (fig. S2) (10). These observations indicate that SAM690 stimulates
13 *Striga* germination by selective activation of ShHTL7 through a mechanism independent of
14 hydrolysis.

15
16 During a series of above assays, we noticed inconsistency in stimulant activities of several
17 SAM690 derivatives depending on the purification method due to active impurity. This
18 byproduct, while only 0.01% of the total product, appeared to be an unusually oxidized
19 molecule that has a hybrid structure resembling SAM690 with a D-ring-like butenolide
20 moiety (Fig. 1A and fig. S3). In order to verify the structure and potency of this derivative,
21 we established a three-step synthetic procedure and the resulting oxygenated SAM690
22 exhibited potency comparable to that of (+)-GR24, as evident from its minimum effective

1 concentration (MEC) of 10 pM (Fig. 1D). As expected from its structure, oxygenated
2 SAM690 was hydrolyzed by ShHTL7 (fig. S2). The structural similarity of this compound
3 to SLs led us to hypothesize that attaching a methyl group to the C4' position may enhance
4 the potency of the molecules. Indeed, this modification improved MEC from 10 pM to 10
5 fM (Fig. 1A and 1D). We named the D-ring/sulfonylpiperazine-hybrid molecule
6 sphynolactone-7 (SPL7) and its demethylated analog H-SPL7 (sulfonylpiperazine hybrid
7 strigolactone mimic of ShHTL7) (stability and toxicology of SPL7 is summarized in fig.
8 S5). The name is derived from the sphinx, a mythical creature with the head of a human
9 and the body of a lion, to represent the hybrid nature of the molecule. The IC₅₀ values of
10 SPL7 improved from SAM690 (0.31 μM vs 8.9 μM) and our LC-MS analysis revealed that
11 SPL7 was hydrolyzed by ShHTL7 to form CLIM at the catalytic histidine residue (Fig. 1E,
12 fig. S2 and S4) (7, 14). The potency of SPL7 is comparable to that of (+)-5-deoxystrigol
13 (5DS), a natural SL that is currently the most potent commercially available germination
14 stimulant for *Striga*.

15
16 Despite their high potencies, the presence of the *N*-arylsulfonylpiperazine scaffold allows
17 SPL7 to retain selectivity towards ShHTL7, whereas 5DS binds to all the SL receptors with
18 different ranges of IC₅₀ values (Fig. 1E) (10). To gain insight into this difference in
19 selectivity, we replaced 16 active site residues of ShHTL7 with those of ShHTL5 (11).
20 Using the YLG binding assay, we identified seven residues essential for the binding with
21 SPL7 (M139, T142, T157, L161, Y174, C194, and M219) (Fig. 2A-B and fig. S6). The
22 combination of these mutations led to a distribution of IC₅₀ values of SPL7, which was

1 correlated with that of H-SPL7 ($R = 0.81$), but not with that of 5DS ($R = 0.15$) (Fig. 2C).
2 These results indicate that SPL molecules utilize a different subset of residues for binding
3 compared to natural SLs, thereby displaying selectivity. Our computational investigation
4 supports the hypothesis that SPL7 could fit to the active site of the homology model of
5 ShHTL7, while changes in polarity and volume through active site mutations may impair
6 its fit (Fig. 2A and fig. S7). These seven amino acids as a combination are unique in
7 *ShHTL7* among known *HTL/KAI2* homologs including those from a parasitic plant
8 *Orobancha minor*, which also utilizes SLs as germination stimulants (fig. S8) (3, 9).
9 Consistently, SPL7 exhibits nM level potency to *O. minor*, and is effective at fM-range for
10 several *S. hermonthica* ecotypes that parasitize to different hosts (fig. S8).
11
12 As SPL7 and GR24 have identical D-ring structures, the selectivity to ShHTL7 and the
13 fM-range potency must be encoded in the ABC-portion of SPL7 (Fig. 3A). In light of an
14 activation model solely dependent on CLIM formation as proposed in D14, the ABC-
15 portion of SPL7 possibly contributes to efficient CLIM formation on the receptor (7, 14).
16 Alternatively, the ABC-portion may have additional functions other than accelerating
17 CLIM formation. We assessed these possibilities through investigation of the relationship
18 between potencies and D-ring hydrolysis using various SPL7 analogs. The potencies of
19 two hydrolysis-resistant analogs, carba-H-SPL7 and 1'-carba-SPL7, were ≥ 100 nM,
20 implying that the hydrolysis of D-ring is dispensable for activity, yet essential to gain the
21 fM-level potency (Fig. 1A and fig. S9). Next, to investigate quantitative relationship
22 between potencies and the hydrolysis reaction rate, we performed a kinetic analysis similar

to that involving surface plasmon resonance, which allows estimation of reaction rate constants k_I and k_{-I} independently (15). Briefly, we obtained the parameter k_I^{CLIM} and $(k_{-I}^{CLIM} + k_2)$ by fitting an equation formularized from a reaction scheme in Fig. 3B to experimentally obtained time-dependent CLIM formation curves (supplementary methods) (8). We assumed $(k_{-I}^{CLIM} + k_2) \approx k_{-I}^{CLIM}$, as observed stability of CLIM-ShHTL7 complex over 30 minutes theoretically limited k_2 to <1% fraction of $(k_{-I}^{CLIM} + k_2)$ in our analysis. The kinetic analysis with SPL7 analogs allowed us to observe only vague trend between potency and k_I^{CLIM} ($R = -0.32$), indicating that the rate of CLIM formation, while important, was not a sole factor for determining potency (Fig. 3B and fig. S10-S11). This interpretation was supported by the observation with GR24, where the reaction rate of the CLIM formation was higher ($k_I^{CLIM} = 316 \times 10^{-3}/\mu\text{M/s}$) than SPL7 ($k_I^{CLIM} = 43.5 \times 10^{-3}/\mu\text{M/s}$) despite a potency 1,000 times lower than that of SPL7 (Fig. 1D and Fig. 3B-C). These results are contradictory to the model proposed for D14, and thus indicating that the ABC-portion of SPL7 has additional functions other than accelerating CLIM formation for delivering the difference in potency (7, 14). Although difference in the uptake or stability in *Striga* seeds could account for differences in potency, we obtained no positive results supporting this assumption (fig. S12). Based on these observations, we hypothesized that the function of the ABC-portion after the hydrolysis is essential to deliver fM-level potency (fig. S13). Verification of this model will require detailed studies on the metabolic fate of SPL7 and crystallization of SPL7-ShHTL7 complex.

We next tested the utility of SPL7 as a *Striga*-selective suicide germination stimulant, using three organism-based bioassays. First, we applied 10 μ M SPL7 to a SL biosynthetic mutant, *more axillary growth4-1* (*max4-1*), to see whether SPL7 restore the increased branching phenotype (16). SPL7 failed to rescue *max4-1* branching defects, while a similar concentration of GR24 did suppress axillary branch emergence (Fig. 4A). SPL7 also failed to induce root hair elongation or induce SL-inducible gene expressions in wild type *Arabidopsis* (Fig. 4B-C) (17, 18). Thus, SPL7 exhibits no hormonal SL activity in *Arabidopsis* assays. Second, we evaluated the effect of SPL7 on AM fungi, which are agronomically important microbes that support the growth of crops. While SLs induced multiple 3° hyphal branches as in *Medicago* root extract, SPL7 exhibited only a mild effect at the highest concentration showing 800 times less activity than (+)-GR24 (Fig. 4D) (19). Lastly, we evaluated the ability of SPL7 to induce suicide germination of *Striga* in a pot infestation assay (Fig. 4E-F). In the DMSO control, *Striga* seeds parasitized maize and emerged from the soil at an average of one seedling per host. Soil treatment with SPL7 at a concentration of 100 pM or higher for a week before planting maize reduced the emergence of *Striga* and protected the host plants from senescence caused by parasitism. In contrast, GR24 requires 10 nM to obtain similar effect. Taken together, we concluded that SPL7 is effective as a *Striga*-selective suicide germination stimulants at least in laboratory experiments.

The discovery of SPL7 reinforced the design principle of SL-mimics as a hybrid of two functional modules, a modifiable synthetic scaffold responsible for both receptor selectivity

1 and potency as the ABC-portion and the D-ring component of natural SLs. Implications of
2 the strategy for basic science includes direct dissection of the roles of specific SL receptors
3 in experimentally intractable organisms like *Striga*. For practical purpose, the strategy
4 appears applicable to other noxious parasitic weeds including *Orobanch*e or *Phelipanche*
5 species.

7 **References:**

- 8 1. G. Ejeta, Integrating New Technologies for *Striga* Control. (World Scientific
9 Publishing, 2007), pp. 3-16.
- 10 2. S. C. Wigchert *et al.*, Dose-response of seeds of the parasitic weeds *Striga* and
11 *Orobanch*e toward the synthetic germination stimulants GR 24 and Nijmegen 1. *J.*
12 *Agric. Food Chem.* **47**, 1705-1710 (1999).
- 13 3. X. Xie, K. Yoneyama, Strigolactone story. *Annu. Rev. Phytopathol.* **48**, 93-117
14 (2010).
- 15 4. K. Akiyama, K. Matsuzaki, H. Hayashi, Plant sesquiterpenes induce hyphal
16 branching in arbuscular mycorrhizal fungi. *Nature* **435**, 824-827 (2005).
- 17 5. T. Arite *et al.*, *d14*, a strigolactone-insensitive mutant of rice, shows an accelerated
18 outgrowth of tillers. *Plant Cell Physiol.* **50**, 1416-1424 (2009).
- 19 6. C. Hamiaux *et al.*, DAD2 is an α/β hydrolase likely to be involved in the perception
20 of the plant branching hormone, strigolactone. *Curr. Biol.* **22**, 2032-2036 (2012).
- 21 7. R. Yao *et al.*, DWARF14 is a non-canonical hormone receptor for strigolactone.
22 *Nature* **536**, 469-473 (2016).

- 1 8. A. de Saint Germain *et al.*, A histidine covalent receptor and butenolide complex
2 mediates strigolactone perception. *Nat. Chem. Biol.* **12**, 787-794 (2016).
- 3 9. C. E. Conn *et al.*, Convergent evolution of strigolactone perception enabled host
4 detection in parasitic plants. *Science* **349**, 540-543 (2015).
- 5 10. Y. Tsuchiya *et al.*, Probing strigolactone receptors in *Striga hermonthica* with
6 fluorescence. *Science* **349**, 864-868 (2015).
- 7 11. S. Toh *et al.*, Structure-function analysis identifies highly sensitive strigolactone
8 receptors in *Striga*. *Science* **350**, 203-207 (2015).
- 9 12. D. Holbrook-Smith, S. Toh, Y. Tsuchiya, P. McCourt, Small-molecule antagonists
10 of germination of the parasitic plant *Striga hermonthica*. *Nat. Chem. Biol.* **12**, 724-
11 729 (2016).
- 12 13. K. Fukui, D. Yamaguchi, S. Ito, T. Asami, A tailor-made design of
13 phenoxyfuranone-type strigolactone mimic. *Front. Plant Sci.* **8**, 1-11 (2017).
- 14 14. R. Yao *et al.*, ShHTL7 is a non-canonical receptor for strigolactones in root
15 parasitic weeds. *Cell Res.* **27**, 838-841 (2017).
- 16 15. R. Karlsson, A. Michaelsson, L. Mattsson, Kinetic analysis of monoclonal antibody-
17 antigen interactions with a new biosensor based analytical system. *J. Immunol. Meth.*
18 **145**, 229–240 (1991).
- 19 16. K. Sorefan *et al.*, *MAX4* and *RMS1* are orthologous dioxygenase-like genes that
20 regulate shoot branching in *Arabidopsis* and pea. *Genes Dev.* **17**, 1469–74 (2003).

17. Y. Kapulnik *et al.*, Strigolactones affect lateral root formation and root-hair elongation in *Arabidopsis*. *Planta*. **233**, 209–216 (2011).
18. D. C. Nelson *et al.*, F-box protein MAX2 has dual roles in karrikin and strigolactone signaling in *Arabidopsis thaliana*. *Proc. Natl. Acad. Sci.* **108**, 8897–8902 (2011).
19. K. Akiyama, S. Ogasawara, S. Ito, H. Hayashi, Structural requirements of strigolactones for hyphal branching in AM fungi. *Plant Cell Physiol.* **51**, 1104-1117 (2010).

References in supplementary materials:

20. I. M. Wallace *et al.*, Compound prioritization methods increase rates of chemical probe discovery in model organisms. *Chem. Biol.* **18**, 1273-1283 (2011).
21. H. Samejima *et al.*, Identification of *Striga hermonthica*-Resistant Upland Rice Varieties in Sudan and Their Resistance Phenotypes. *Front. Plant Sci.* **7**, 1-12 (2016).
22. H. Samejima *et al.*, Practicality of the suicidal germination approach for controlling *Striga hermonthica*. *Pest Manag. Sci.* **72**, 2035-2042 (2016).
23. H. Norén, P. Svensson, B. Anderson, A convenient and versatile hydroponic cultivation system for *Arabidopsis thaliana*. *Physiol. Plant* **121**, 343-348 (2004).
24. A. Bordoli *et al.*, The SWISS-MODEL workspace: A web-based environment for protein structure homology modelling. *Bioinformatics* **22**, 195-201 (2006).
25. M. A. Larkin *et al.*, Clustal W and Clustal X version 2.0. *Bioinformatics* **23**, 2947-2948 (2007).

- 26 E. Harder *et al.*, OPLS3: A force field providing broad coverage of drug-like small
molecules and proteins. *J. Chem. Theory Comput.* **22**, 195-201 (2015).
27. T. A. Halgaren *et al.*, Glide: A new approach for rapid, accurate docking and
scoring. 2. Enrichment Factors in Database Screening. *J. Med. Chem.* **47**, 1750-
1759 (2004).
28. W. Sherman *et al.*, Novel procedure for modeling ligand/receptor induced fit
effects. *J. Med. Chem.* **49**, 534-553 (2006).
29. S. Schnell, C. Mendoza, Closed Form Solution for Time-dependent Enzyme
Kinetics. *J. Theor. Biol.* **187**, 207-212 (1997).
30. Computer code MAPLE, Waterloo Maple Inc., Waterloo, Ontario, Canada,
<https://www.maplesoft.com/>

Acknowledgments:

We thank A. Babiker, S. Runo, and P. Matana for providing the *S. hermonthica* seeds, K. Yoneyama for providing *O. minor* seeds, and S. Hagihara and M. Yoshimura for providing YLG. We thank N. Nakamichi for instructing RT-qPCR analysis and J.X. Yap for supporting biochemistry works. We thank A. Miyazaki for proof reading. **Authors contributions:** The chemical aspect of the research was managed by D.U. and T.O. Conceptualization of the project and the management of biological aspect of the research was performed by Y.T. Chemical screening was performed by Y.T. under the supervision of P.M. and T.K. Y.T. and H.I. performed *Striga* germination assays and YLG assays. S.A.M. synthesized analog series of initial hits, and R.Y. synthesized SPL7 analogs under

the supervision of D.U. and T.O. Arabidopsis assays, RT-qPCR, and suicide germination assay were performed by H.I. under supervision of Y.T. N.M. performed hyphal branching assay with AM fungi under the supervision of K.A. K.K. performed LC- MS analyses for small molecules and proteins. Mathematical characterization of CLIM formation was performed by Y.H. Homology model and docking simulations were performed by C.R. under supervision of S.I. Y.T. wrote the overall story of the manuscript. The manuscript was edited by D.U., P.M., T.K. and T.O. All the authors discussed for the manuscript.

Funding: This work was supported by a Grant in Aid for Scientific Research from the Ministry of Education, Culture, Sports, Science, and Technology (15KT0031 and 15K07102 to Y.T. and 15H059556 to T.K.), and a grant from the Advanced Low Carbon Technology Research and Development Program from the Japan Science and Technology Agency (T.K.). Support for CR from the Japan Society for the Promotion of Science (JSPS) and the Alexander von Humboldt Foundation (AvH) is gratefully acknowledged. P.M. were funded by the Natural Sciences and Engineering Research Council of Canada (NSERC). ITbM is supported by the World Premier International Research Center Initiative (WPI), Japan. **Competing interests:** Nagoya U. has filed for patents regarding the following topics: “Regulators for germination in *Striga* species” Inventors: Tsuchiya, Y., Uruguchi, D., Sathiyarayanan, AM, Hagihara, S., Yoshimura, M., Kinoshita, T., Ooi, T., and Itami, K. (patent publication no. WO 2017/002898 and JP 2017-014149); “Regulators for germination in parasitic plants”. Inventors: Tsuchiya, Y., Uruguchi, D., Ooi, T., Kinoshita, T. and Kuwata, K. (patent application no. PCT/JP2018/36785 and JP 2017-193773). We declare no financial conflicts of interest in relation to this work. **Data and materials**

availability: All data are available in the manuscript or the supplementary material. The complete sets of raw data underlying all figures in the main text and supplement can be found in the Supplementary Materials.

Supplementary Materials:

Materials and Methods

Table S1

Figures S1-S13

References (20-30)

Figure legends:

Fig. 1. Development of a femtomolar-range germination stimulant for *Striga*. (A)

Scheme of structure development. MEC represents the lowest concentration of compound that produces any seed germination. **(B)** SAM690 induces *Striga* seed germination at 10 μ M. Bar = 1 mm. **(C)** 10 μ M aminoethoxyvinyl glycine (AVG) suppresses (+)-GR24 and SAM690. **(D)** *Striga* germination in dilution series of SPL7, H-SPL7, 5DS, and (+)-GR24. **(E)** Competitive bindings to ShHTLs and AtD14. IC₅₀ value (μ M) in the YLG assay is presented as a heat map with s.d. ($n = 3$ technical replicates). Data for 5DS was obtained from (10). Error bars in (C) and (D) indicate s.d. ($n = 3$ biological replicates).

Fig. 2. Active-site residues differentiating selectivity of SPL7 and 5DS. (A) Homology models of ShHTL7 and its septuple mutant with mutated amino acids located in the active sites. Brown circles indicate polar to non-polar mutations. The yellow circle indicates reduction of the pocket volume by T157Y. (B) IC_{50} values (μM) in the YLG assay with the mutant series of ShHTL7. Sixteen active-site residues were replaced with those corresponding to ShHTL5. Quadruple, hextuple, and septuple mutants are shown with s.d. ($n = 3$ technical replicates). (C) Distribution of IC_{50} values (μM) in the series of ShHTL7 mutants.

Fig. 3. Mode of action of SPL7. (A) Annotation of structural modules identified from the structure–activity–relationship study. (B) Relationship between reaction rate constants and MEC among SPL7 analogs. Reaction scheme (top) and scatter plot of k_I^{CLIM} or k_{-I}^{CLIM} against MEC of *Striga* germination (bottom) are presented. (C) Time-dependent CLIM formation quantified by LC-MS. T_{50} indicates the half-maximal time. Error bar indicates s.d. ($n = 3$ technical replicates).

Fig. 4. Bioassays with SPL7. (A) SPL7 does not suppress shoot branching phenotype of *Arabidopsis* SL biosynthetic mutant, *max4-1*, at 10 μM . Arrows indicate axillary branches. Average numbers of axillary branches are indicated with s.e. n indicates number of plants tested. Bar = 5 cm. (B) SPL7 fails to enhance root hair elongation in *Arabidopsis* wild-type at 10 μM . Average length of root hair is presented with s.d. ($n = 7$ biological replicates). Bar = 100 μm . (C) SPL7 fails to induce SL-inducible *BRANCHED1* (*BRC1*) expression in

1 *Arabidopsis* wild-type at 10 μ M. Average expression obtained from quantitative RT-PCR
2 analysis is presented as relative value to DMSO control with s.d. ($n = 3$, biological
3 replicates). **(D)** SPL7 shows 800-fold lower potency for AM fungi than that of (+)-GR24.
4 MEC represents the lowest concentration of compound that induces multiple 3° hyphae.
5 Data for (+)-GR24 were obtained from (19). Bar = 1 mm. **(E)** Suicide germination assay.
6 Representative pictures taken after 2 months (left) or 3 months (right) of co-cultivation of
7 maize with *Striga*. The soil was pre-treated with DMSO or 10 nM of SPL7. Arrows
8 indicate emerged *Striga*. Bar = 5 cm. **(F)** Number of emerged *Striga* after 2 months of co-
9 cultivation. n indicates number of hosts tested. Error bar indicates s.e.

10

Figure 1

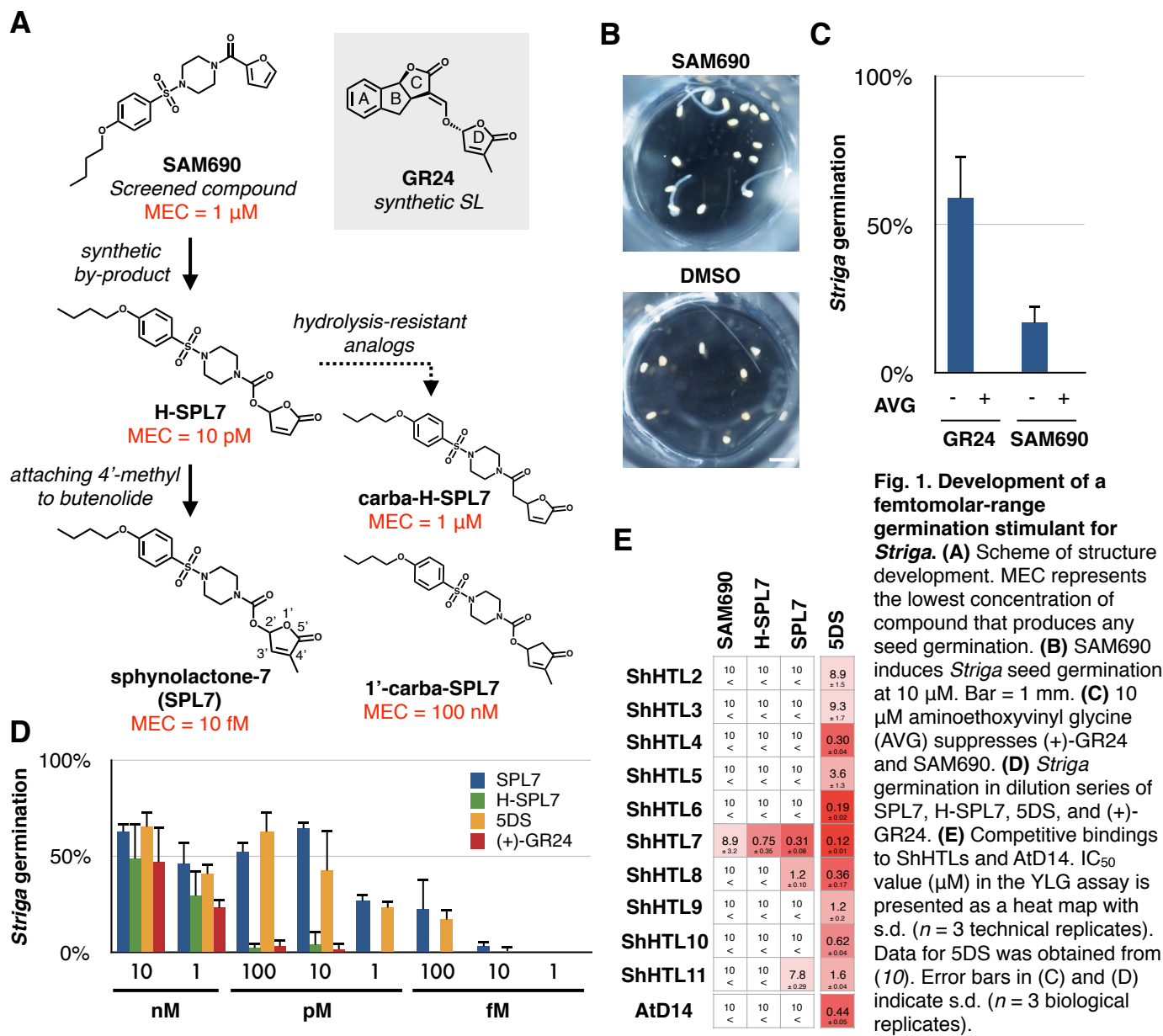


Fig. 1. Development of a femtomolar-range germination stimulant for *Striga*. (A) Scheme of structure development. MEC represents the lowest concentration of compound that produces any seed germination. (B) SAM690 induces *Striga* seed germination at 10 μ M. Bar = 1 mm. (C) 10 μ M aminoethoxyvinyl glycine (AVG) suppresses (+)-GR24 and SAM690. (D) *Striga* germination in dilution series of SPL7, H-SPL7, 5DS, and (+)-GR24. (E) Competitive bindings to ShHTLs and AtD14. IC₅₀ value (μ M) in the YLG assay is presented as a heat map with s.d. ($n = 3$ technical replicates). Data for 5DS was obtained from (10). Error bars in (C) and (D) indicate s.d. ($n = 3$ biological replicates).

Figure 2

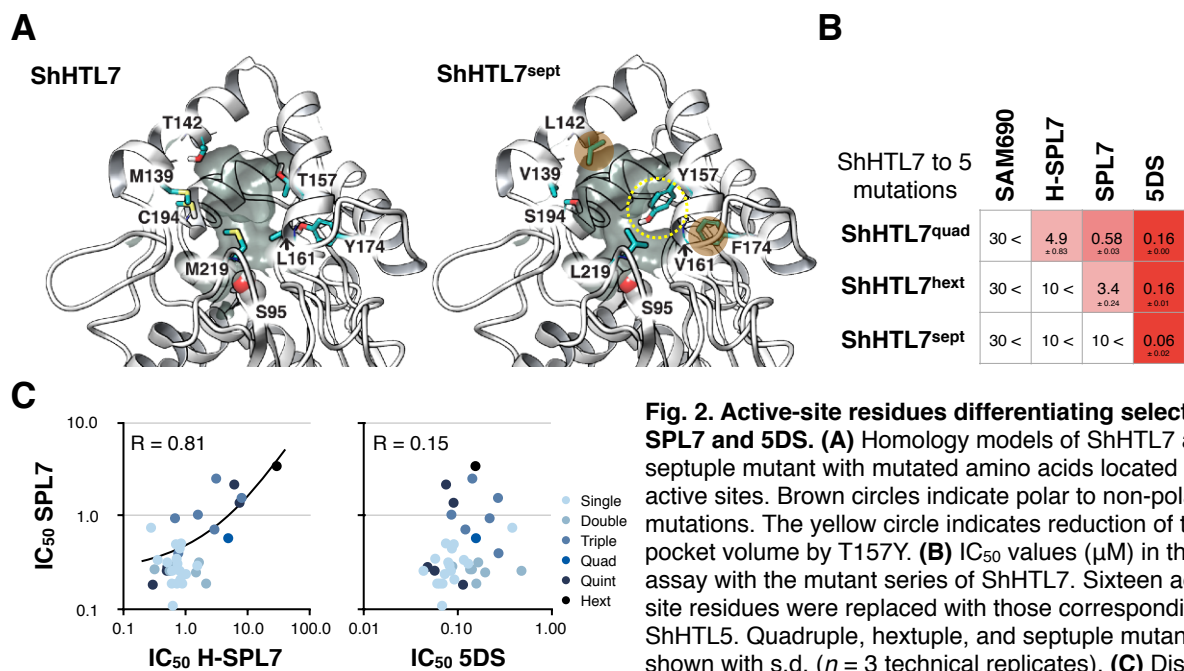


Fig. 2. Active-site residues differentiating selectivity of SPL7 and 5DS. (A) Homology models of ShHTL7 and its septuple mutant with mutated amino acids located in the active sites. Brown circles indicate polar to non-polar mutations. The yellow circle indicates reduction of the pocket volume by T157Y. (B) IC₅₀ values (μM) in the YLG assay with the mutant series of ShHTL7. Sixteen active-site residues were replaced with those corresponding to ShHTL5. Quadruple, hextuple, and septuple mutants are shown with s.d. (n = 3 technical replicates). (C) Distribution of IC₅₀ values (μM) in the series of ShHTL7 mutants.

Figure 3

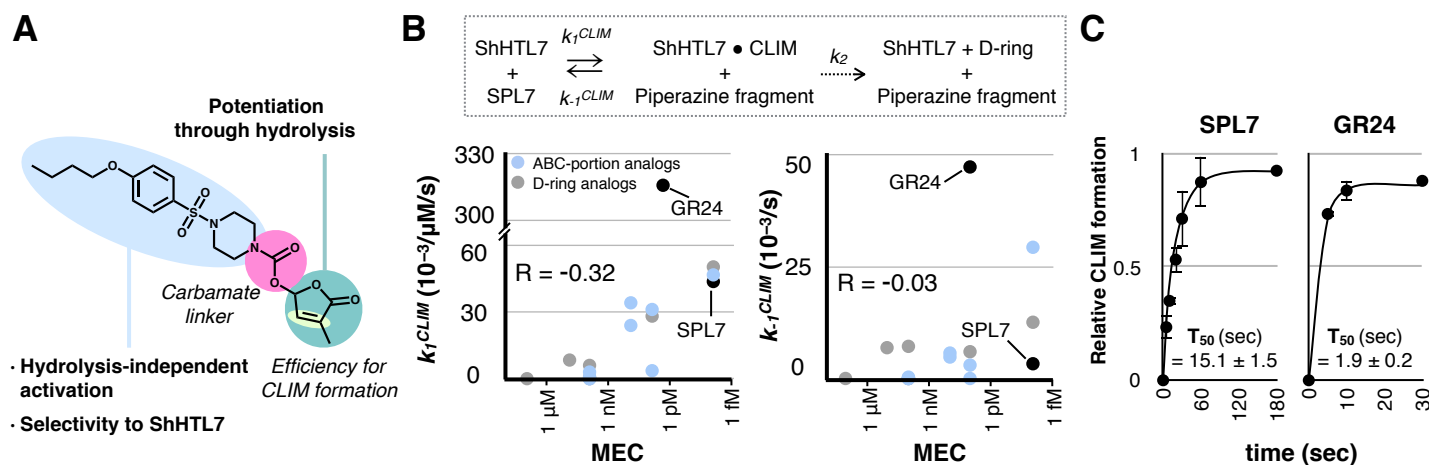


Fig. 3. Mode of action of SPL7. (A) Annotation of structural modules identified from the structure–activity–relationship study. (B) Relationship between reaction rate constants and MEC among SPL7 analogs. Reaction scheme (top) and scatter

plot of k_1^{CLIM} or k_{-1}^{CLIM} against MEC of *Striga* germination (bottom) are presented. (C) Time-dependent CLIM formation quantified by LC-MS. T_{50} indicates the half-maximal time. Error bar indicates s.d. ($n = 3$ technical replicates).

Figure 4

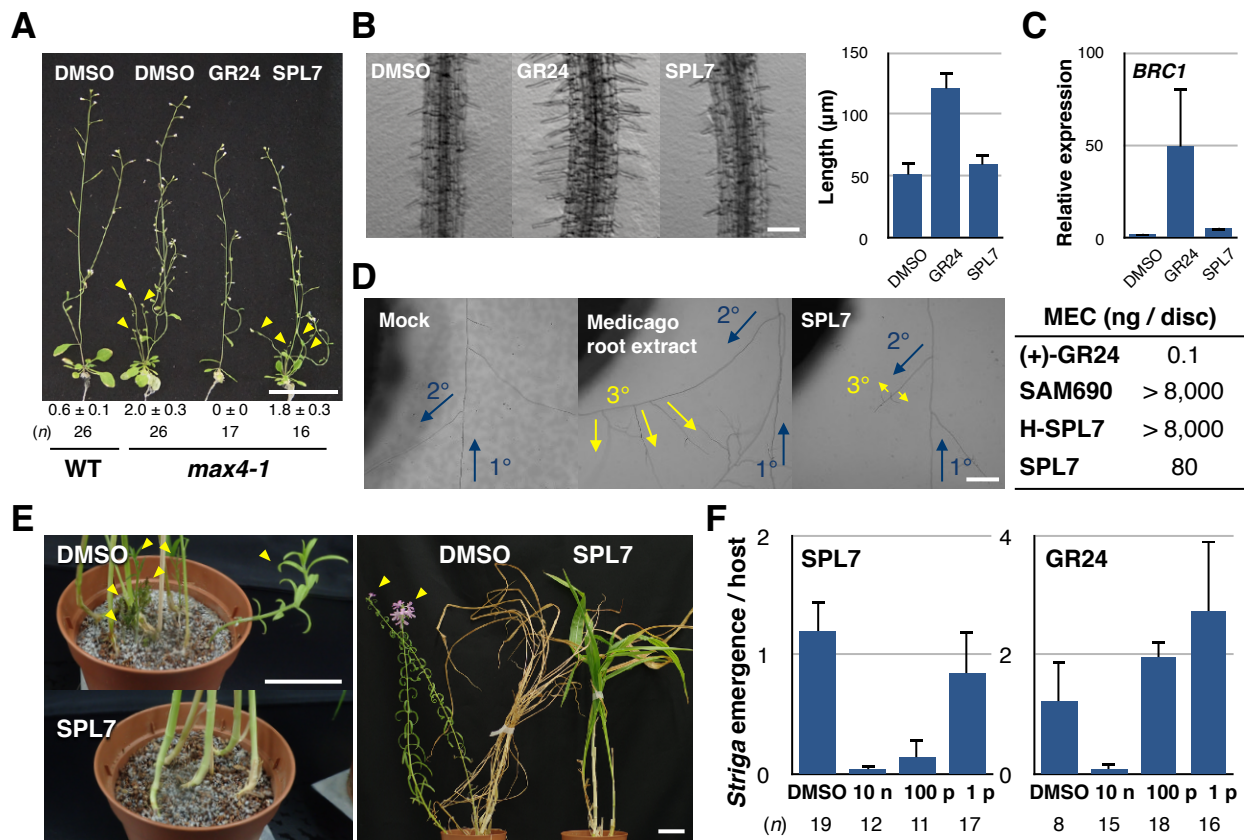


Fig. 4. Bioassays with SPL7. (A) SPL7 does not suppress shoot branching phenotype of *Arabidopsis* SL biosynthetic mutant, *max4-1*, at 10 μ M. Arrows indicate axillary branches. Average numbers of axillary branches are indicated with s.e. *n* indicates number of plants tested. Bar = 5 cm. (B) SPL7 fails to enhance root hair elongation in *Arabidopsis* wild-type at 10 μ M. Average length of root hair is presented with s.d. (*n* = 7 biological replicates). Bar = 100 μ m. (C) SPL7 fails to induce SL-inducible *BRANCHED1* (*BRC1*) expression in *Arabidopsis* wild-type at 10 μ M. Average expression obtained from quantitative RT-PCR analysis is presented as relative value to

DMSO control with s.d. (*n* = 3, biological replicates). (D) SPL7 shows 800-fold lower potency for AM fungi than that of (+)-GR24. MEC represents the lowest concentration of compound that induces multiple 3° hyphae. Data for (+)-GR24 were obtained from (19). Bar = 1 mm. (E) Suicide germination assay. Representative pictures taken after 2 months (left) or 3 months (right) of co-cultivation of maize with *Striga*. The soil was pre-treated with DMSO or 10 nM of SPL7. Arrows indicate emerged *Striga*. Bar = 5 cm. (F) Number of emerged *Striga* after 2 months of co-cultivation. *n* indicates number of hosts tested. Error bar indicates s.e.

Science



Supplementary Materials for

A femto-molar range suicide germination stimulant for the parasitic plant
Striga hermonthica

Daisuke Uraguchi, Keiko Kuwata, Yuh Hijikata, Rie Yamaguchi, Hanae Imaizumi,
Sathiyarayanan AM, Christin Rakers, Narumi Mori, Kohki Akiyama, Stephan Irle, Peter
McCourt, Toshinori Kinoshita, Takashi Ooi, Yuichiro Tsuchiya

Correspondence to: uraguchi@chembio.nagoya-u.ac.jp, tooi@chembio.nagoya-u.ac.jp,
yuichiro@itbm.nagoya-u.ac.jp

This PDF file includes:

Materials and Methods
Figs. S1 to S13
Table S1

Materials and Methods

Germination assay

Germination assays in *Striga* were described previously (10). Unless specified, we used *Striga hermonthica* seeds collected from plants growing on sorghum in the Gadaref State Eastern Sudan. *S. hermonthica* seeds from Mbutu region in Tanzania (harvested from mixed stands of sorghum, finger millet and maize field) or Alupe region in Kenya (harvested from maize fields) were used for germination assay in fig. S8. All experiments using *Striga* were conducted under permissions from the plant protection station of the Japanese Ministry of Agriculture. For *Orobancha minor* germination assay, dry seeds were first washed with small amount of chloroform to remove wax on the seed coat, followed by surface sterilization with 20% commercial bleach for 10 min. After extensive wash with sterilized MilliQ water, the seeds were conditioned at room temperature on moist blotting paper for two weeks in the dark. The procedure after conditioning was identical to that for *S. hermonthica* except for the incubation at room temperature.

Chemical screening

A total of 12,000 synthetic small molecules from the Yeast Active (20) and Tripos libraries (Tripos Discovery Research) were screened in 96-well plates for germination of *Striga*. Around 30 seeds/well were treated with library small molecules at concentration of 25 μ M in 100 μ L of MilliQ water with the final concentration of 1% DMSO for 2 days and germination was monitored under a microscope. The screening was performed in duplicate

1 and small molecules reproducibly stimulated *Striga* germination were selected as initial
2 hits.

3 4 Suicide germination assay

5 The pot suicide germination assay was developed by modifying methods reported by
6 Samejima *et al.* (21, 22). Plastic pots (130-mm diameter, 113-mm depth, perforated at the
7 bottom) were filled with 0.7 L of dry autoclaved soil composed of equal amounts of
8 vermiculite and compost. Then, 5 mg of *S. hermonthica* seeds were mixed into the top 5 cm
9 of the soil, watered from bottom, covered with a plastic bag and conditioned at 30 °C for 11
10 days. The soil was treated with 350 mL of distilled water containing SPL7 or (+)-GR24
11 with 0.0001% DMSO, followed by an additional 6-day incubation. Five maize seeds were
12 sown in each pot after it was uncovered. All pots were watered from the bottom at 2–3-days
13 intervals throughout the growing period (about 3 months). The number of *Striga* plants that
14 emerged per pot was counted after 2 months of co-cultivation under constant light
15 condition at 30°C and divided by the number of germinated hosts. S.d. was calculated from
16 replication experiments in 3 pots for DMSO control or 5 pots for small molecule
17 treatments.

18 19 *Arabidopsis* phenotype assays

20 Our growth room for *Arabidopsis* was set under a 16 h white light (50 $\mu\text{mol m}^{-2} \text{s}^{-1}$)/8 h
21 dark cycle at 24 °C under relative humidity of 55-70%. For shoot branching assay in
22 *Arabidopsis*, wild-type (Col-0) and *max4-1* seeds were surface sterilized with 20%

commercial bleach in 70% ethanol, rinsed with ethanol, and dried on a clean bench. The seeds were incubated on agar media containing $0.5 \times$ Murashige-Skoog (MS) salts for 18 days. The seedlings were transferred to a plastic plate floater and grown on hydroponic culture containing (+)-GR24 or SPL7 at $10 \mu\text{M}$ concentration (0.1% DMSO) for 3 weeks (23). The container was covered with plastic wrap until the apical shoot reached it. The number of axillary buds (1 cm or longer) was counted 20 days after transferred to hydroponic culture. For root hair assay, seeds of Col-0 were surface-sterilized and germinated on $0.5 \times$ MS plates containing $10 \mu\text{M}$ GR24, $10 \mu\text{M}$ SPL7 (both initially dissolved in DMSO) or equal amount of DMSO (0.1%) as control. Plates were kept vertically in the dark at 4°C for 2 days then incubated in the growth room, tilted by approximately 60 degrees for 13 days. Pictures of roots were taken under a microscope (ZEISS stemi 508) equipped with a WRAYMER WRAYCAM NOA 2000. Root-hair length was measured using ImageJ2 (<https://imagej.net/ImageJ2>) and presented as average of 5 root hairs per a plant. Average length from 7 plants with s.d. is shown in Fig. 4B.

Hyphal branching assay in AM-fungi

Hyphal branching activity on germinating spores of *Gigaspora margarita* Becker & Hall (MAFF 520054) was evaluated as reported previously (4). Test samples were first dissolved in chloroform at concentration of $800 \mu\text{g/mL}$ then serially diluted with ethyl acetate. After being loaded with test sample solutions ($10 \mu\text{L}$), paper discs (6 mm in diameter; ADVANTEC) were dried by placing on a filter paper at room temperature for at least 1 h, and then placed in front of the tips of the secondary hyphae. The hyphal branch

patterns were observed 24 h after treatment. The control was mock-treated with solvent-dried paper discs. An ethyl acetate-soluble neutral fraction prepared from root exudates of *Medicago truncatula* was used as a positive control.

YLG assay

YLG is commercially available from Tokyo Chemical Industry (#E1238). Protein expression and an *in vitro* competition assay with YLG were performed as described previously (10). Site-specific mutation to *ShHTL7* in p15TV-L was introduced by PCR. For the high-throughput assay shown in fig. S1B, a single concentration of 10 μ M of each analog was tested. IC₅₀ values were calculated through fitting of a sigmoid curve in ImageJ2.

RNA extraction and quantitative RT-qPCR

Seeds of Col-0 were surface-sterilized and germinated on 0.5 \times MS plates containing 0.1% DMSO. Six-day seedlings were transferred to 0.5 \times MS plates containing 10 μ M (+)-GR24, 10 μ M SPL7 or 0.1% DMSO. After 24 h, total RNAs were extracted and purified using illustra RNAspin Mini (GE Healthcare). Each RNA sample was prepared from 6 whole seedlings. Reverse transcription from 450 ng of total RNA was carried out using ReverTra Ace (TOYOBO) according to the instruction provided by the manufacture. qPCR was performed using the Power SYBER Green PCR Master Mix and StepOnePlus Real-Time PCR system (Applied Biosystems). For gene-specific amplifications of BRC1 transcripts, the following primer set was used: 5'-CCAGTGATTAACCACCATCG-3' (forward) and

5'-TGCATGAGGTCTCTTGGTTT-3' (reverse) (18). Relative quantification was carried out using comparative cycle threshold method using *ISOPENTENYL PYROPHOSPHATE: DIMETHYLALLYL PYROPHOSPHATE ISOMERASE 2 (IPP2)* gene transcripts, which are amplified with the primers 5'-GAGACGTCTCATCATGTTTGAGGATG-3' (forward) and 5'-GGAGAAGCAACTCATACTTCGAG-3' (reverse), as an initial control. The relative expression level to the DMSO-treated seedlings is shown in Fig. 4C.

Small molecule analysis by LC-MS

Hydrolysis reaction analysis: 1 μ M of SPL7 analog was reacted with 1 μ g of 6 \times His-tagged ShHTL7 in reaction buffer (100 mM HEPES, 150 mM NaCl, pH 7.0) at final volume of 100 μ L for 30 min, and the reaction mixture was injected to a Dionex Ultimate 3000 HPLC system by an autosampler (Thermo Fisher Scientific). The HPLC system was interfaced with an Exactive Plus Fourier transfer mass spectrometer (Thermo Fisher Scientific) with an electrospray ionization source. The chromatography mobile phases were solvent A (aqueous 0.1% formic acid) and solvent B (acetonitrile). The column was developed at a flow rate of 200 μ L min⁻¹ with the following concentration gradient of acetonitrile: from 5% B to 95% B in 10 min, hold at 95% B for 2 min, from 95% B to 5% B in 0.1 min, and finally, re-equilibrate at 2% B for 7 min. The electrospray ionization source was operated in positive ion mode. Data acquisition and analysis were performed through Xcalibur software (version 2.2). A PLRP-S column (3 μ m, 2.1 \times 150 mm, Agilent) was used. **Quantification of uptake in *Striga* seeds:** Mixture of SPL7 and (+)-GR24 (10 nM each) were incubated with 50 mg of conditioned *Striga* seeds in 1 mL distilled water for 1

h. After 3 times of washes with distilled water, small molecules were extracted from the seeds with 1 mL of acetone overnight. The acetone extract was split into two aliquots and 2 pmol of the two small molecules were added to one of them as an internal standard. Quantification was carried out by measuring peak area relative to that corresponding to 2 pmol. The acetone extracts were concentrated *in vacuo* prior to LC-MS analysis. **Stability of SPL7, (+)-GR24, and 5DS under various pH conditions:** The three small molecules were mixed in single HPLC vial at the final concentration of 1 μ M (1% DMSO) in following aqueous buffers at 100 mM; potassium phosphate (pH 5.5 or 6.5), HEPES (pH 7.0, 7.5 or 8.2) or Tris (pH 9.0). The time course of degradation was monitored by LC-MS analysis using an Inertsil ODS-5 column (ϕ 2.1 \times 100 mm, 5 μ m, COSMOSIL, nakalai tesque), eluted by a linear gradient from 5 to 90% acetonitrile in water containing 0.1% formic acid within 3 min at a flow rate of 0.3 mL min⁻¹. Compounds eluted from the column were detected with an ESI positive ion mode. Peak area corresponding to these small molecules were measured and presented as relative value to t = 0.

Quantification of time-dependent CLIM formation

For quantification of CLIM formation, 0.6 μ M ShHTL7 protein was reacted with 1 μ M SPL7 analogs in reaction buffer (100 mM HEPES, 150 mM NaCl, pH 7.0) at 100 μ L scale for the indicated reaction time at room temperature. The reaction was stopped by adding trifluoroacetic acid to the final concentration at 1%. The mixture was centrifuged (25 $^{\circ}$ C, 15,000 rpm, 5 min), and the supernatant was used for LC-MS analysis. The HPLC condition was modified from the method for the hydrolysis reaction analysis as a flow rate

of 0.3 mL min⁻¹ with the following concentration gradient of acetonitrile: from 5% B to 95% B in 5 min. Quantification was carried out by measuring peak area of ShHTL7 and ShHTL7·CLIM ($z = 29$) using ImageJ2, and the relative value of ShHTL7·CLIM against total protein (ShHTL7 + ShHTL7·CLIM) is presented in Fig. 3C and fig. S10-11. The obtained data was used for kinetic analysis.

Mass spectrometric analysis of covalent modification via digestion in solution

ShHTL7 protein was reacted with (+)-GR24 or SPL7 for 30 min as described above. The reaction mixture was diluted with 8 M urea (dissolved in 250 mM ammonium bicarbonate; ABC), reduced with 25 mM TCEP, alkylated with 12.5 mM iodoacetamide and digested by LysC (Wako pure chemical). After the solution was diluted with ABC (in order to reduce the concentration of urea below 2 M), digestion with trypsin (Promega) was carried out at 37 °C overnight. The reaction was stopped by adding trifluoroacetic acid to a final concentration of 0.4%, and the pH of the solution was adjusted to <2. The solution was desalted through GL-Tip SDB micropipette tips (GL Science), dried, and then re-dissolved in 0.1% trifluoroacetic acid. For LC-MS/MS analysis, peptides were separated using a 115-min gradient elution at a flow rate of 0.5 μ L min⁻¹ with a Thermo-Dionex Ultimate 3000 HPLC system (Thermo Fisher Scientific), which was directly interfaced with a Q Exactive mass spectrometer (Thermo Fisher Scientific). A capillary C18 reverse phase column (NTCC-360/100-3-125, 125 \times 0.1 mm, Nikkyo Technos) was used as the analytical column. Mobile phase A consisted of 0.5% acetic acid, and mobile phase B consisted of 80% acetonitrile and 0.5% acetic acid, with the following concentration gradient of

1 acetonitrile: from 5% B to 40% B in 100 min, 40% B to 95% B in 0.1 min, hold at 95% B
2 for 3 min, from 95% B to 5% B in 0.1 min, and finally re-equilibrate with 5% B for 12 min.
3 The Q Exactive mass spectrometer was operated in the data-dependent acquisition mode
4 using Xcalibur 4.0 software, with a single full-scan mass spectrum in the Orbitrap (350–
5 1,800 m/z , 70,000 resolution) followed by 10 data-dependent MS/MS scans in the Orbitrap
6 at 35% normalized collision energy (HCD) = 27. MS/MS spectra from each LC-MS/MS
7 run were queried against the ShHTL7 protein database using the Proteome Discoverer
8 (Version 2.2) search algorithm. The search criteria were as follows: full tryptic specificity
9 was required, two missed cleavages were allowed, carbamidomethylation (C) was set as a
10 fixed modification, oxidation (M) and substitution of a proton with D-ring ($\Delta MS = 96.0211$
11 Da ($C_5H_4O_2$)) (H, K, S, T) were set as a variable modification, the precursor ion mass
12 tolerance was 10 ppm for all MS acquired in the Orbitrap mass analyzer, and the fragment
13 ion mass tolerance was 0.02 Da for all MS/MS spectra acquired in the Orbitrap. A high-
14 confidence score filter (FDR <1%) was used to select the “hit” peptides, and their
15 corresponding MS/MS spectra were manually inspected.

16 17 Molecular modeling

18 Based on the Protein Data Bank (PDB) entry 5CBK for *Striga* receptor ShHTL5
19 (monomeric X-ray structure with 2.46 Å resolution), a homology model of ShHTL7 was
20 constructed using the SWISS-MODEL server (11, 24). The sequence similarity between the
21 two proteins is 68.89%, and the structural alignment of homology model between ShHTL7
22 and ShHTL5 had a 0.49 Å root-mean-square deviation. Sequence alignments were

performed through the EBI ClustalW web server (25). The homology model of ShHTL7 was further refined and minimized using the OPLS3 force field as implemented in the SCHRÖDINGER suite (Small-Molecule Drug Discovery Suite 2017-4, Schrödinger) (26). The final model was then evaluated using the UCLA metaserver SAVES (Structural Analysis and Verification Server; <https://services.mbi.ucla.edu/SAVES/>), obtaining ERRAT and VERIFY3D quality factors of 98.1 and 95.2%, respectively. The obtained QMEAN score (model reliability) from SWISS-MODEL (24) was 0.77. Based on the final model, mutants of ShHTL7 were constructed and minimized for further computational investigations. In all *in silico* simulations, histidine 246 was assumed to be in the “HID” state (i.e. hydrogen present on the δ -nitrogen of histidine) to ensure potential hydrogen bonding with serine 95 of the catalytic triad His-Ser-Asp of ShHTLs. The 3D structures of small molecules including 5DS and SPL7 derivatives were built using SMILES, processed through SCHRÖDINGER’s ligand preparation protocol and docked via Glide into the receptors (ShHTL5, ShHTL7, and ShHTL7sept-mutant), utilizing induced fit docking protocols with default settings (27, 28).

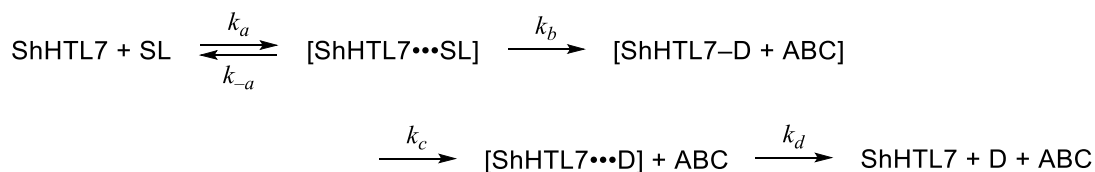
Kinetic analysis of the hydrolysis reaction

The activation of the SL receptors is a dynamic process with a series of steps involving the ligand hydrolysis reaction. The current receptor-activation model in D14, in which the formation of CLIM triggers the conformational change of the receptor, is proposed based on a crystallographic study of D14/MAX2 complex and LC-MS detection of the existence of CLIM (7, 8, 14). However, these static data do not allow us to distinguish whether the

CLIM formation is the trigger of the receptor activation or is a consequence of the receptor activation. To gain insight into the process from a dynamic point of view, we performed a kinetic analysis of the CLIM formation reactions between ShHTL7 and SPL7 analogs. We anticipated that, by fitting experimentally obtained reaction curves of time-dependent CLIM formation to a reaction kinetic model, we will be able to obtain reaction rate constants for each analog. If there is a rate-limiting step in the activation of ShHTL7, obtained constants corresponding to the step may correlate with the physiological activity of the analogs.

1. Modeling the hydrolysis reaction of strigolactone

We observed that SPL7 analogs gave variable time-dependent reaction curves with unique reaction rates (represented by T_{50}) and steady-state levels (fig. S10- S11). For example, replacement of piperazine in SPL7 to 7-membered ring slowed down T_{50} from 15.1 seconds to 3.3 min without changing the steady state level. By contrast, modification of 4'-methyl in the D-ring of SPL7 to 4'-butyl reduced the steady state level by one half. To gain deeper insights into the relationship between reaction curves and stimulant activities, we first constructed a reaction scheme of the enzymatic hydrolysis reaction of SL, referring to previously proposed scheme as follows (8).



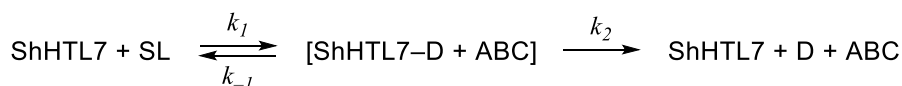
[ShHTL7 \cdots SL]: complex of ShHTL7 and SL without a covalent bond

[ShHTL7-D]: complex of ShHTL7 and D-ring with a covalent bond (CLIM)

[ShHTL7 \cdots D]: complex of ShHTL7 and D-ring without covalent bond

Scheme 1. The hydrolysis reaction of SL in ShHTL7. In the SL = SPL7 case, ABC corresponds to the *N*-sulfonylpiperazine fragment.

The k_x ($x = a, -a, b, c, d$) values indicate kinetic constants for the above reaction steps. Theoretically, it is essential to quantify all the intermediate state molecules in order to obtain all the five constants in Scheme 1. As it is impossible at this moment to estimate all five kinetic constant values from experiment, we simplified Scheme 1 by splitting it into two parts before and after the covalent adduct (CLIM) formation between ShHTL7 and the D-ring. Consequently, Scheme 1 was rewritten as shown in Scheme 2.



Scheme 2. Simplified hydrolysis reaction of SL in ShHTL7.

The k_1 , k_2 , and k_{-1} in Scheme 2 correspond to $\min(k_a, k_b)$ and $\min(k_c, k_d)$, and the k_a in Scheme 1, respectively. Description of $[\text{ShHTL7-D}]_t$ by the initial concentration of $[\text{ShHTL7}]_0$, $[\text{SL}]_0$, and two parameters, K and k_1 , under quasi-initial condition ($[\text{SL}]_t \approx$

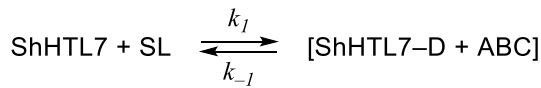
[SL]₀) led an analogous equation to that used in a kinetic analysis of ligand-receptor interactions by surface plasmon resonance (SPR) as below (15),

$$[ShHTL7 - D]_t = \frac{[ShHTL7]_0[SL]_0}{K+[SL]_0} \{1 - e^{-(K+[SL]_0)k_1 t}\}, K = \frac{k_{-1}+k_2}{k_1} \text{ (Eq. 1).}$$

The parameters of k_1 and K can be obtained by fitting the equation to the experimental time evolution data $[ShHTL7-D]_t$, and $(k_{-1} + k_2)$ can be obtained by multiplying K with k_1 .

Under the assumption that the release rate of CLIM from ShHTL7 is slow (approximation of $k_2 = 0$), $(k_{-1} + k_2)$ reduces to k_{-1} . This analysis is different from the Michaelis Menten scheme where the dependency of $[SL]_0$ on the reaction rate is analyzed under the quasi-steady state (QSS) approximation.

We could obtain Eq. 1 by another approach with further simplification of Scheme 2. Under the assumption of $k_2 = 0$, Scheme 2 can be simplified as shown in Scheme 3 below.



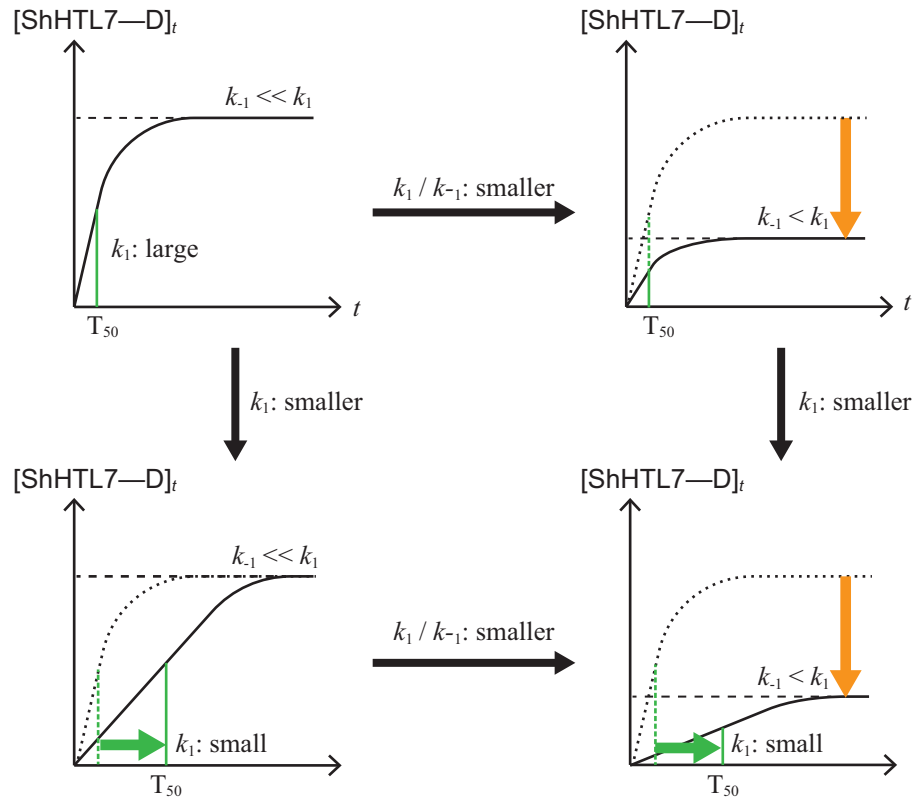
Scheme 3. Further simplified hydrolysis reaction of SL in ShHTL7.

Scheme 3 (Eq. 1) can be formulated to Eq. 2 below,

$$[ShHTL7 - D]_t = \frac{[ShHTL7]_0[SL]_0}{\frac{k_{-1}}{k_1} + [SL]_0} \left\{ 1 - e^{-\left(\frac{k_{-1}}{k_1} + [SL]_0\right)k_1 t} \right\} \quad (\text{Eq. 2}).$$

Eq. 2 is identical to Eq. 1 with k_2 substituted with 0, thus revealing that Eq. 1 is compatible with Scheme 3.

Based on Eq. 1, variations in T_{50} values and steady-state levels can be expressed with the difference in k_1 and k_{-1} under the approximation of $k_2 = 0$ as shown in Scheme 4.



Scheme 4. Relationship between kinetic constants and reaction curve

Scheme 4 denotes that the kinetic constant k_1 is a determining factor of T_{50} values. The ratio of k_1 to k_{-1} is a determining factor of the level of [ShHTL7-D] at equilibrium state.

We approximated $k_2 = 0$ based on the observation that CLIM from all the SPL7 analogs were stable over 30 min, which indicates that k_2 values are small. To rationalize this approximation, we estimated hypothetical values of k_2 that give the half-life period of [ShHTL7-D]_t ($t_{1/2}$) as 30 min (a hypothetical condition where the release of CLIM goes faster than the real condition). If the hypothetical k_2 values compose only a small fraction of the sum ($k_{-1} + k_2$), real k_2 values should compose even a smaller fraction of the total, and thus our assumption of $k_2 = 0$ is rationalized. The hypothetical k_2 values were obtained by the equation, $k_2 = \ln(2) / t_{1/2}$ based on the second step in Scheme 2. Relative k_2 values to total ($k_{-1} + k_2$) are shown below (the analogs are corresponding to those in fig. S10 and S11).

D-ring analogs	SPL7	Et-SPL7	H-SPL7	ⁿ Bu-SPL7	ⁱ Bu-SPL7	3'Me-H-SPL7	3'Me-SPL7	Bn-SPL7	sat-H-SPL7	
$\frac{k_2}{(k_{-1} + k_2)} \times 10^5$	11.7	3.1	6.5	5.3	5.5	962.7	n.d	n.d	n.d	
ABC-portion analogs	Im-SPL7	Diazepine-SPL7	Bz-SPL7	ⁿ HexSO ₂ -SPL7	ⁱ PrSO ₂ -SPL7	Ms-SPL7	pPent-SPL7	pMeO-SPL7	pPentO-SPL7	GR24
$\frac{k_2}{(k_{-1} + k_2)} \times 10^5$	8.2	256.7	770.2	137.5	385.1	n.d	1.3	12.8	6.8	0.8

All the obtained relative values of k_2 were $<1\%$ of total fraction even in the hypothetical conditions. We therefore concluded that our approximation of $k_2 = 0$ is reasonable, as experimentally obtained k_2 value should occupy smaller than 1% fraction of $(k_{-1} + k_2)$.

2. Derivation of fitting equation

Based on the Scheme 2, we can obtain nonlinear differential equations (the reaction rate equations) as follows:

$$\frac{d[ShHTL7]_t}{dt} = -k_1[ShHTL7]_t[SL]_t + k_{-1}[ShHTL7 - D]_t + k_2[ShHTL7 - D]_t,$$

$$\frac{d[ShHTL7-D]_t}{dt} = k_1[ShHTL7]_t[SL]_t - k_{-1}[ShHTL7 - D]_t - k_2[ShHTL7 - D]_t,$$

$$\frac{d[P]_t}{dt} = k_2[ShHTL7 - D]_t,$$

$$\frac{d[SL]_t}{dt} = -k_1[ShHTL7]_t[SL]_t + k_{-1}[ShHTL7 - D]_t,$$

where $[X]_t$ ($X = ShHTL7, SL, ShHTL7-D, P$, and SL) denotes the concentration of X at time t , and P is either D or ABC . According to the conservation law, we obtain the following equations:

$$[ShHTL7]_0 = [ShHTL7]_t + [ShHTL7 - D]_t,$$

$$[SL]_0 = [SL]_t + [ShHTL7 - D]_t + [P]_t.$$

[ShHTL7-D]₀ under the quasi-initial condition ([SL]_t ≈ [SL]₀) can be described as follows
(29):

$$[ShHTL7 - D]_t = \frac{[ShHTL7]_0[SL]_0}{K+[SL]_0} \{1 - e^{-(K+[SL]_0)k_1 t}\}, K = \frac{k_{-1}+k_2}{k_1} \quad (\text{Eq. 1}).$$

We employed these equations to analyze measured [ShHTL7-D]_t data. *K* and *k₁* are fitting parameters, and fitting of the equation to the measured [ShHTL7-D]_t analysis was performed using Fit function in statistics package in Maple 18 (30). After obtaining *K* and *k₁* through fitting, we estimated *k₋₁* under the assumption that *k₂* = 0, which was rationalized in the modeling section.

3. Limitations

Despite the similarity to the kinetic analysis involving SPR, our analysis employed specific conditions and simplifications to analyze the unique reaction between SLs and ShHTL7.

We assume that our analysis involves the following general or specific limitations.

I. Quantification of CLIM formation in the time-dependent manner is essential.

As with SPR, our analysis applies to experimental procedures where direct measurement of ligand-receptor complex (equivalent to a substrate-enzyme complex [ES] in Michaelis Menten kinetics) are possible. Those with products [P] as outputs are not applicable to this analysis.

II. The analysis is not applicable to distinguish reaction processes.

1 Although the obtained k_1 value represents the smaller value between rate of ligand-
2 receptor binding or hydrolysis reaction rate, distinguishing these two processes is out
3 of the scope of the analysis due to the simplification in Scheme 2.

4 III. CLIM-receptor complex must be stable.

5 The analysis estimates reaction rate constants under an ideal condition where release of
6 CLIM from ShHTL7 does not occur ($k_2 = 0$). Precautions should be taken to interpret
7 obtained k_1 value with careful consideration of the reasonability of k_2 . Notably, in the
8 case when it takes long time to reach the steady-state (when k_1 is small), the
9 significance of k_2 could be nonnegligible even when the release of CLIM is slow.

10 IV. Precise knowledge of reaction time is critical.

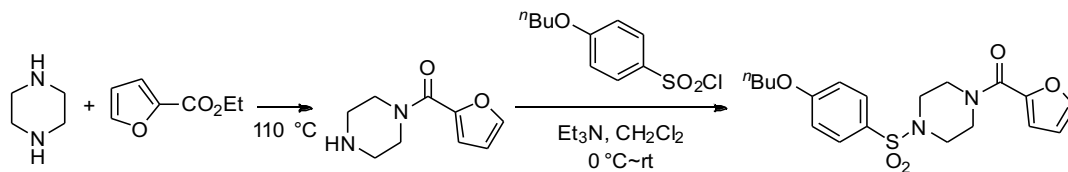
11 Since Eq. 1 includes the variable t as a reciprocal of the exponent, experimental errors
12 in reaction time are exponentially amplified. Thus, precision in the values for the
13 reaction time relative to the experimental time scale is critical to obtain reliable results.
14 For example, in a reaction where a ligand quickly reacts with ShHTL7 and reaches to
15 steady levels (when k_1 is large), small timing errors in measurements amplify errors in
16 the fitting parameter k_1 and consequently K .

18 Chemical synthesis

19 *General Information:* Infrared spectra were recorded on a Shimadzu IRAffinity-1
20 spectrometer. ^1H NMR spectra were recorded on a JNM-ECZ400S (400 MHz, JEOL) or
21 JNM-ECA600II (600 MHz, JEOL) spectrometer. Chemical shifts are reported in ppm,
22 using tetramethylsilane (0.0 ppm) resonance (CDCl_3) or solvent resonance (acetone- d_6 ;

2.05 ppm) as the internal standard. Data are reported as follows: chemical shift, integration, multiplicity (s = singlet, d = doublet, t = triplet, q = quartet, m = multiplet, br = broad) and coupling constant (Hz). ¹³C NMR spectra were recorded on a JNM-ECS500 (121 MHz, JEOL) or JNM-ECA600II (151 MHz, JEOL) spectrometer with complete proton decoupling. Chemical shifts are reported in ppm, using solvent resonance as the internal standard (acetone-*d*₆; 29.84 ppm, CDCl₃; 77.16 ppm). High-resolution mass spectra were obtained using Exactive (Thermo Fisher Scientific) for electrospray ionization (ESI). Analytical thin layer chromatography (TLC) was performed on precoated TLC plates (silica gel 60 GF₂₅₄, 0.25 mm, Merck). Flash column chromatography was conducted on silica gel 60 (spherical, 40–50 μm; Kanto Chemical), silica gel 60N (spherical, 40–50 μm; Kanto Chemical), and PSQ60AB (spherical, av. 55 μm; Fuji Silysia Chemical). Recycling preparative HPLC was performed using HPLC LC-forte/R (YMC) equipped with a silica gel column [φ 20 mm × 250 mm, YMC-Pack SIL SL12S05-2520WT]. Dichloromethane (CH₂Cl₂) and tetrahydrofuran (THF) were supplied from Kanto Chemical in “dehydrated” form and further purified by passage through neutral alumina under a nitrogen atmosphere. Other simple chemicals were purchased and used without purification.

Procedure for the preparation of SAM690:

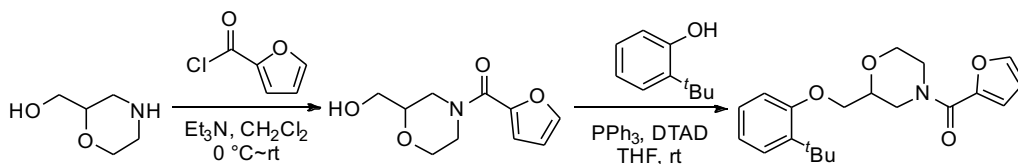


1 A mixture of piperazine (516.8 mg, 6.0 mmol) and ethyl furan-2-carboxylate (280.3
2 mg, 2.0 mmol) was melted at 110 °C under argon atmosphere and stirred for 3 h. The
3 reaction mixture was then diluted with CH₂Cl₂ (20 mL) and washed with 0.5 M
4 hydrochloric acid. The aqueous layer was adjusted to pH 10 using an aqueous solution of
5 K₂CO₃ and extracted with CHCl₃ three times. The combined organic extracts were dried
6 over Na₂SO₄, and concentrated. The residue was purified by column chromatography
7 (CHCl₃/MeOH as eluent) to furnish the requisite furan-2-yl(piperazin-1-yl)methanone in
8 53% yield (191.0 mg, 1.06 mmol) as a syrupy liquid. **Furan-2-yl(piperazin-1-**
9 **yl)methanone:** ¹H NMR (600 MHz, CDCl₃) δ 7.48 (1H, brs), 6.98 (1H, d, *J* = 3.6 Hz), 6.48
10 (1H, dd, *J* = 3.6, 1.5 Hz), 3.78 (4H, br), 2.93 (4H, t, *J* = 5.1 Hz), N-H proton was not found
11 probably due to broadening; ¹³C NMR (151 MHz, CDCl₃) δ 159.4, 148.1, 143.7, 116.4,
12 111.4, 46.5, one carbon atom was not found probably due to broadening; IR (film) 3453,
13 3298, 3109, 2913, 2850, 1609, 1568, 1483, 1429, 1275, 1184, 1141, 1120, 1013, 945 cm⁻¹;
14 HRMS (ESI) Calcd for C₉H₁₂O₂N₂Na⁺ ([M+Na]⁺) 203.0791, Found 203.0790.

15 A solution of furan-2-yl(piperazin-1-yl)methanone (191.0 mg, 1.06 mmol), 4-
16 butoxybenzenesulfonyl chloride (289.8 mg, 1.17 mmol), and triethylamine (0.22 mL, 1.59
17 mmol) in CH₂Cl₂ (4 mL) was stirred at 0 °C~ambient temperature overnight and the
18 reaction was then quenched by adding a saturated aqueous solution of NaHCO₃. The
19 aqueous phase was extracted with CH₂Cl₂ three times. The combined organic phases were
20 washed with a saturated aqueous solution of NaCl and dried over Na₂SO₄. After filtration,
21 removal of volatiles under reduced pressure followed by purification of the residue on a
22 silica gel column (hexane/ethyl acetate as eluent) furnished SAM690 in 80% yield (332.8

mg, 0.85 mmol). **SAM690**: ^1H NMR (400 MHz, CDCl_3) δ 7.67 (2H, d, $J = 8.7$ Hz), 7.45 (1H, brs), 7.00 (1H, d, $J = 4.0$ Hz), 6.98 (2H, d, $J = 8.7$ Hz), 6.97 (1H, s), 6.47 (1H, dd, $J = 3.2, 2.0$ Hz), 4.02 (2H, t, $J = 6.7$ Hz), 3.90 (4H, br), 3.05 (4H, t, $J = 5.1$ Hz), 1.80 (2H, quintet, $J = 6.7$ Hz), 1.51 (2H, sextet, $J = 6.7$ Hz), 0.99 (3H, t, $J = 6.7$ Hz); ^{13}C NMR (121 MHz, CDCl_3) δ 163.1, 159.0, 147.6, 144.1, 130.0, 126.4, 117.4, 115.0, 111.7, 68.3, 46.3, 31.2, 19.3, 13.9, one carbon atom was not found probably due to overlapping; IR (film) 2958, 2932, 2871, 1623, 1594, 1486, 1430, 1346, 1263, 1160, 1110, 1010, 942 cm^{-1} ; HRMS (ESI) Calcd for $\text{C}_{19}\text{H}_{24}\text{O}_5\text{N}_2\text{NaS}^+$ ($[\text{M}+\text{Na}]^+$) 415.1298, Found 415.1294.

Procedure for the preparation of SAM-M10:



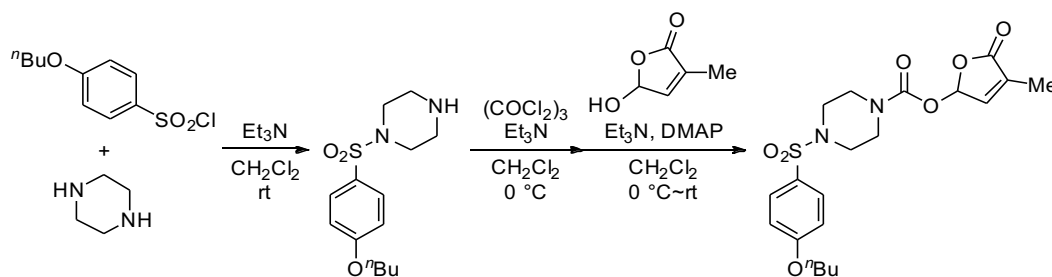
To a solution of 2-morpholinemethanol (315.9 mg, 2.7 mmol) and triethylamine (0.45 mL, 3.2 mmol) in CH_2Cl_2 (10 mL) was added 2-furoyl chloride (0.27 mL, 2.7 mmol) at 0 °C. The reaction mixture was stirred at 0 °C~ambient temperature overnight and quenched by adding a saturated aqueous solution of NaHCO_3 . The aqueous phase was extracted with CH_2Cl_2 three times. The combined organic phases were washed with a saturated aqueous solution of NaCl and dried over Na_2SO_4 . After filtration, evaporation of the solvent followed by purification of the residue on a silica gel column (hexane/ethyl acetate as eluent) furnished furan-2-yl(2-(hydroxymethyl)morpholino)methanone in 60% yield (341.8 mg, 1.62 mmol) as a colorless oil. **Furan-2-yl(2-**

(hydroxymethyl)morpholino)methanone: ^1H NMR (400 MHz, CDCl_3) δ 7.49 (1H, dd, J = 1.8, 0.9 Hz), 7.05 (1H, dd, J = 3.5, 0.9 Hz), 6.50 (1H, dd, J = 3.5, 1.8 Hz), 4.43 (2H, brd, J = 12.8 Hz), 4.01 (1H, dd, J = 11.6, 2.4 Hz), 3.78-3.59 (4H, m), 3.20 (2H, br), 1.99 (1H, m); ^{13}C NMR (151 MHz, CDCl_3) δ 159.4, 147.8, 144.0, 117.1, 111.6, 76.1, 66.8, 63.6, 46.7, 44.5; IR (film) 3406, 2923, 2860, 1611, 1485, 1433, 1279, 1184, 1115, 1070, 1037, 886 cm^{-1} ; HRMS (ESI) Calcd for $\text{C}_{10}\text{H}_{13}\text{O}_4\text{NNa}^+$ ($[\text{M}+\text{Na}]^+$) 234.0737, Found 234.0737.

To a stirred solution of furan-2-yl(2-(hydroxymethyl)morpholino)methanone (19.0 mg, 0.09 mmol), triphenylphosphine (28.8 mg, 0.11 mmol), and 2-*tert*-butylphenol (16.8 μL , 0.11 mmol) in THF (3 mL) was added di-*tert*-butyl azodicarboxylate (DTAD, 25.3 mg, 0.11 mmol) in THF (0.1 mL) dropwise and the resulting mixture was stirred at ambient temperature for 48 h. The reaction mixture was quenched by adding water and extracted with ethyl acetate. The organic layer was then washed with a saturated aqueous solution of NaCl, dried and concentrated in vacuo. The residue obtained was purified by silica gel column chromatography (hexane/ethyl acetate as eluent) to furnish SAM-M10 in 16% yield (4.95 mg, 0.014 mmol) as a viscous liquid. **SAM-M10:** ^1H NMR (600 MHz, CDCl_3) δ 7.47 (1H, brs), 7.29 (1H, dd, J = 8.4, 1.5 Hz), 7.18 (1H, td, J = 8.4, 1.5 Hz), 7.06 (1H, d, J = 3.6 Hz), 6.92 (1H, t, J = 8.4 Hz), 6.86 (1H, d, J = 8.4 Hz), 6.49 (1H, dd, J = 3.6, 1.2 Hz), 4.75 (1H, d, J = 12.6 Hz), 4.47 (1H, brd, J = 12.6 Hz), 4.13 (1H, dd, J = 9.3, 4.5 Hz), 4.08-3.99 (2H, m), 3.99-3.94 (1H, m), 3.72 (1H, td, J = 11.4, 1.8 Hz), 3.25 (2H, br), 1.38 (9H, s); ^{13}C NMR (151 MHz, CDCl_3) δ 159.4, 157.2, 147.8, 144.0, 138.2, 127.2, 126.9, 121.0, 117.2, 112.0, 111.5, 74.3, 68.4, 66.9, 50.0, 42.9, 34.9, 30.0; IR (film) 2954, 2915, 2863, 1623,

1 1489, 1429, 1269, 1231, 1181, 1122, 1055, 1032, 941 cm^{-1} ; HRMS (ESI) Calcd for
2 $\text{C}_{20}\text{H}_{25}\text{O}_4\text{NNa}^+$ ($[\text{M}+\text{Na}]^+$) 366.1676, Found 366.1675.

3
4 *Representative procedure for the preparation of SPL7:*

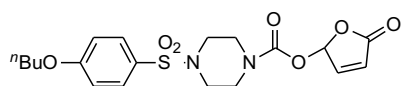


6 To a solution of piperazine (0.19 g, 2.2 mmol) in CH_2Cl_2 (5.4 mL) were added 4-
7 butoxybenzenesulfonyl chloride (0.13 g, 0.54 mmol) and triethylamine (0.11 mL, 0.81
8 mmol) at ambient temperature. The reaction mixture was stirred for 18 h and quenched by
9 addition of a saturated aqueous solution of NaHCO_3 . The aqueous phase was extracted with
10 CH_2Cl_2 three times and the combined organic extracts were dried over Na_2SO_4 . After
11 concentration, the residue was purified by column chromatography ($\text{CHCl}_3/\text{MeOH}$ as
12 eluent) to afford 4-butoxyphenyl(piperazin-1-yl)sulfone in 93% yield (0.15 g, 0.5 mmol) as
13 a white solid. **4-Butoxyphenyl(piperazin-1-yl)sulfone:** ^1H NMR (600 MHz, CDCl_3) δ
14 7.67 (2H, d, $J = 9.0$ Hz), 6.98 (2H, d, $J = 9.0$ Hz), 4.02 (2H, t, $J = 7.2$ Hz), 2.96 (4H, t, $J =$
15 4.8 Hz), 2.92 (4H, t, $J = 4.8$ Hz), 1.80 (2H, quintet, $J = 7.2$ Hz), 1.57-1.45 (4H, m), 0.99
16 (3H, t, $J = 7.2$ Hz), N-H proton was not found probably due to broadening; ^{13}C NMR (151
17 MHz, CDCl_3) δ 162.8, 130.0, 126.9, 114.7, 68.3, 47.1, 45.5, 31.2, 19.3, one carbon atom
18 was not found probably due to broadening; IR (film) 2952, 2930, 2872, 1593, 1576, 1497,

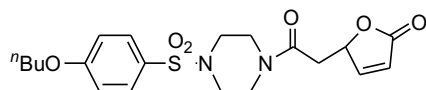
1 1468, 1339, 1256, 1153, 1095, 942, 876 cm^{-1} ; HRMS (ESI) Calcd for $\text{C}_{14}\text{H}_{22}\text{O}_3\text{N}_2\text{NaS}^+$
2 ($[\text{M}+\text{Na}]^+$) 321.1243, Found 321.1243.

3 4-Butoxyphenyl(piperazin-1-yl)sulfone (0.15 g, 0.50 mmol) and triethylamine (0.2
4 mL, 1.50 mmol) were introduced to a solution of triphosgene (0.15 g, 0.50 mmol) in
5 CH_2Cl_2 (1.9 mL) at 0°C under argon atmosphere and the solution was stirred for 2 h. A
6 solution of 5-hydroxyfuran-2(5*H*)-one (0.17 g, 1.5 mmol), triethylamine (0.2 mL, 1.50
7 mmol), and *N,N*-dimethyl-4-aminopyridine (DMAP, 6.1 mg, 0.05 mmol) in CH_2Cl_2 (5.0
8 mL) was added to the resulting mixture at 0°C . The reaction mixture was allowed to
9 gradually warm up to ambient temperature during 18 h of stirring. The reaction was
10 quenched upon addition of a saturated aqueous solution of NaHCO_3 and the aqueous phase
11 was extracted with CH_2Cl_2 three times. The combined organic extracts were dried over
12 Na_2SO_4 and concentrated to afford the crude residue. Purification of the residue was
13 performed by silica gel column chromatography (hexane/ethyl acetate as eluent) to furnish
14 0.19 g of SPL7 in 87% yield (190.7 mg, 0.44 mmol) as a white solid. **SPL7**: ^1H NMR (600
15 MHz, CDCl_3) δ 7.65 (2H, dt, $J = 9.0, 1.8$ Hz), 6.99 (2H, dt, $J = 9.0, 1.8$ Hz), 6.85-6.83 (1H,
16 m), 6.83-6.82 (1H, m), 4.03 (2H, t, $J = 6.0$ Hz), 3.76 (1H, d, $J = 12.0$ Hz), 3.65 (1H, d, $J =$
17 12.0 Hz), 3.47 (1H, t, $J = 10.2$ Hz), 3.43 (1H, t, $J = 10.2$ Hz), 3.19 (1H, br), 3.12 (1H, br),
18 2.84 (1H, t, $J = 10.2$ Hz), 2.79 (1H, t, $J = 10.2$ Hz), 1.97 (3H, s), 1.80 (2H, td, $J = 7.2, 6.0$
19 Hz), 1.51 (2H, sextet, $J = 7.2$ Hz), 0.99 (3H, t, $J = 7.2$ Hz); ^{13}C NMR (151 MHz, CDCl_3) δ
20 171.1, 163.2, 152.4, 142.1, 134.7, 130.0, 126.4, 115.0, 93.9, 68.4, 45.8, 43.7, 43.4, 31.2,
21 19.3, 14.0, 10.8, one carbon atom was not found due to overlapping; IR (film) 2940, 2872,

1 1776, 1717, 1593, 1435, 1346, 1242, 1159, 1092, 1015, 955, 930 cm^{-1} ; HRMS (ESI) Calcd
2 for $\text{C}_{20}\text{H}_{26}\text{O}_7\text{N}_2\text{NaS}^+$ ($[\text{M}+\text{Na}]^+$) 461.1353, Found 461.1356.

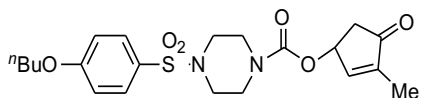


5 **H-SPL7:** ^1H NMR (600 MHz, CDCl_3) δ 7.65 (2H, d, $J = 9.0$ Hz), 7.27 (1H, d, $J = 6.0$ Hz),
6 6.99 (2H, d, $J = 9.0$ Hz), 6.96 (1H, m), 6.28 (1H, d, $J = 6.0$ Hz), 4.03 (2H, t, $J = 7.2$ Hz),
7 3.76 (1H, d, $J = 10.2$ Hz), 3.66 (1H, d, $J = 10.8$ Hz), 3.49 (1H, t, $J = 9.0$ Hz), 3.44 (1H, t, J
8 $= 9.0$ Hz), 3.19 (1H, br), 3.12 (1H, br), 2.85 (1H, t, $J = 9.0$ Hz), 2.81 (1H, t, $J = 9.0$ Hz),
9 1.80 (2H, quintet, $J = 7.2$ Hz), 1.51 (2H, sextet, $J = 7.2$ Hz), 0.99 (3H, t, $J = 7.2$ Hz); ^{13}C
10 NMR (151 MHz, CDCl_3) δ 169.6, 163.2, 152.2, 149.7, 130.0, 126.4, 125.5, 115.0, 95.4,
11 68.4, 45.8, 43.7, 43.5, 31.2, 19.3, 13.9, one carbon atom was not found due to overlapping;
12 IR (film) 2961, 2934, 2872, 1792, 1719, 1595, 1435, 1348, 1242, 1161, 1092 cm^{-1} ; HRMS
13 (ESI) Calcd for $\text{C}_{19}\text{H}_{24}\text{O}_7\text{N}_2\text{NaS}^+$ ($[\text{M}+\text{Na}]^+$) 447.1196, Found 447.1193.

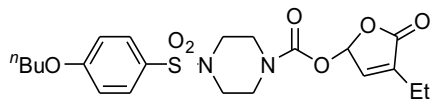


16 **carba-H-SPL7:** ^1H NMR (600 MHz, CDCl_3) δ 7.66 (2H, d, $J = 8.7$ Hz), 7.65 (1H, d, $J =$
17 6.0 Hz), 7.00 (2H, d, $J = 8.7$ Hz), 6.10 (1H, d, $J = 6.0$ Hz), 5.42 (1H, t, $J = 6.0$ Hz), 4.03
18 (2H, t, $J = 7.2$ Hz), 3.81-3.78 (1H, m), 3.64-3.59 (1H, m), 3.56-3.46 (2H, m), 3.11-3.03
19 (2H, m), 2.98-2.90 (3H, m), 2.49 (1H, dd, $J = 16.2, 8.4$ Hz), 1.80 (2H, quintet, $J = 7.2$ Hz),
20 1.51 (2H, sextet, $J = 7.2$ Hz), 0.99 (3H, t, $J = 7.2$ Hz); ^{13}C NMR (151 MHz, CDCl_3) δ
21 172.5, 166.7, 163.2, 156.8, 130.0, 126.4, 121.8, 115.0, 79.9, 68.4, 46.1, 45.9, 45.2, 41.1,

36.9, 31.2, 19.3, 13.9; IR (film) 2959, 2929, 2873, 1786, 1757, 1647, 1595, 1498, 1465,
1448, 1346, 1260, 1160, 1096 cm^{-1} ; HRMS (ESI) Calcd for $\text{C}_{20}\text{H}_{26}\text{O}_6\text{N}_2\text{NaS}^+$ ($[\text{M}+\text{Na}]^+$)
445.1404, Found 445.1396.

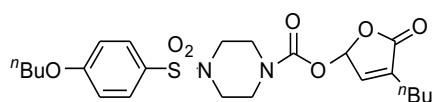


1'-carba-SPL7: ^1H NMR (600 MHz, CDCl_3) δ 7.66 (2H, d, $J = 8.7$ Hz), 7.16 (1H, br), 6.99
(2H, d, $J = 8.7$ Hz), 5.65 (1H, br), 4.02 (2H, t, $J = 7.2$ Hz), 3.70-3.45 (4H, m), 3.10-2.84
(4H, br), 2.81 (1H, dd, $J = 19.2, 6.0$ Hz), 2.29 (1H, dd, $J = 19.2, 1.8$ Hz), 1.81 (3H, s), 1.80
(2H, quintet, $J = 7.2$ Hz), 1.51 (2H, sextet, $J = 7.2$ Hz), 0.99 (3H, t, $J = 7.2$ Hz); ^{13}C NMR
(151 MHz, CDCl_3) δ 205.2, 163.1, 154.3, 153.0, 145.7, 130.0, 126.6, 114.9, 71.7, 68.4,
45.9, 43.5, 43.2, 41.6, 31.2, 19.3, 13.9, 10.2, one carbon atom was not found probably due
to overlapping; IR (film) 2958, 2932, 2872, 1696, 1594, 1498, 1458, 1430, 1347, 1241,
1158, 1125, 1088, 986, 924 cm^{-1} ; HRMS (ESI) Calcd for $\text{C}_{21}\text{H}_{28}\text{O}_6\text{N}_2\text{NaS}^+$ ($[\text{M}+\text{Na}]^+$)
459.1560, Found 459.1548.

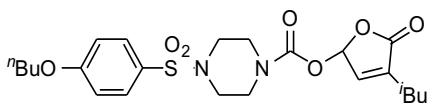


Et-SPL7: ^1H NMR (600 MHz, CDCl_3) δ 7.65 (2H, d, $J = 9.0$ Hz), 6.99 (2H, d, $J = 9.0$ Hz),
6.85-6.83 (1H, m), 6.81-6.80 (1H, m), 4.03 (2H, t, $J = 6.6$ Hz), 3.76 (1H, d, $J = 12.6$ Hz),
3.67 (1H, d, $J = 12.6$ Hz), 3.48 (1H, t, $J = 9.6$ Hz), 3.44 (1H, t, $J = 9.6$ Hz), 3.19 (1H, t, $J =$
6.6 Hz), 3.13 (1H, t, $J = 6.6$ Hz), 2.84 (1H, t, $J = 9.6$ Hz), 2.79 (1H, t, $J = 9.6$ Hz), 2.34 (2H,

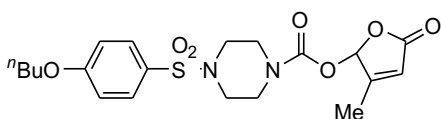
q, $J = 7.4$ Hz), 1.80 (2H, quintet, $J = 6.6$ Hz), 1.51 (2H, sextet, $J = 6.6$ Hz), 1.18 (3H, t, $J = 7.4$ Hz), 0.99 (3H, t, $J = 6.6$ Hz); ^{13}C NMR (151 MHz, CDCl_3) δ 170.7, 163.2, 152.4, 140.7, 140.6, 130.0, 126.4, 115.0, 94.1, 68.4, 45.8, 43.7, 43.4, 31.2, 19.3, 18.9, 13.9, 11.5, one carbon atom was not found due to overlapping; IR (film) 2961, 2936, 2874, 1778, 1721, 1595, 1464, 1435, 1350, 1242, 1161, 1125, 1092, 1020, 947 cm^{-1} ; HRMS (ESI) Calcd for $\text{C}_{21}\text{H}_{28}\text{O}_7\text{N}_2\text{NaS}^+$ ($[\text{M}+\text{Na}]^+$) 475.1509, Found 475.1505.



***n*Bu-SPL7:** ^1H NMR (600 MHz, CDCl_3) δ 7.65 (2H, d, $J = 7.8$ Hz), 6.99 (2H, d, $J = 7.8$ Hz), 6.83 (1H, br), 6.80 (1H, br), 4.03 (2H, t, $J = 7.2$ Hz), 3.76 (1H, d, $J = 12.3$ Hz), 3.66 (1H, d, $J = 12.3$ Hz), 3.47 (1H, t, $J = 9.9$ Hz), 3.44 (1H, t, $J = 9.9$ Hz), 3.18 (1H, brs), 3.12 (1H, brs), 2.84 (1H, t, $J = 9.0$ Hz), 2.79 (1H, t, $J = 9.0$ Hz), 2.31 (2H, t, $J = 7.8$ Hz), 1.80 (2H, quintet, $J = 7.2$ Hz), 1.55 (2H, quintet, $J = 7.2$ Hz), 1.51 (2H, sextet, $J = 7.2$ Hz), 1.37 (2H, sextet, $J = 7.2$ Hz), 0.99 (3H, t, $J = 7.2$ Hz), 0.93 (3H, t, $J = 7.2$ Hz); ^{13}C NMR (151 MHz, CDCl_3) δ 170.8, 163.2, 152.4, 141.1, 139.3, 129.9, 126.4, 115.0, 94.0, 68.4, 45.8, 43.6, 43.4, 31.2, 29.3, 25.0, 22.4, 19.3, 13.9, 13.8, one carbon atom was not found due to overlapping; IR (film) 2957, 2932, 2872, 1776, 1717, 1593, 1497, 1433, 1348, 1240, 1159, 1092, 1015, 955 cm^{-1} ; HRMS (ESI) Calcd for $\text{C}_{23}\text{H}_{32}\text{O}_7\text{N}_2\text{NaS}^+$ ($[\text{M}+\text{Na}]^+$) 503.1822, Found 503.1802.

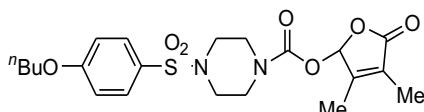


1Bu-SPL7: ^1H NMR (600 MHz, CDCl_3) δ 7.65 (2H, d, $J = 9.0$ Hz), 6.99 (2H, d, $J = 9.0$ Hz), 6.85 (1H, s), 6.83-6.81 (1H, m), 4.03 (2H, t, $J = 7.2$ Hz), 3.76 (1H, d, $J = 12.6$ Hz), 3.66 (1H, d, $J = 12.6$ Hz), 3.48 (1H, t, $J = 9.9$ Hz), 3.44 (1H, t, $J = 9.9$ Hz), 3.19 (1H, br), 3.13 (1H, br), 2.84 (1H, t, $J = 8.4$ Hz), 2.79 (1H, t, $J = 8.4$ Hz), 2.22 (1H, dd, $J = 16.2, 7.2$ Hz), 2.19 (1H, dd, $J = 16.2, 7.2$ Hz), 1.93 (1H, nonet, $J = 7.2$ Hz), 1.80 (2H, quintet, $J = 7.2$ Hz), 1.51 (2H, sextet, $J = 7.2$ Hz), 0.99 (3H, t, $J = 7.2$ Hz), 0.94 (6H, d, $J = 7.2$ Hz); ^{13}C NMR (151 MHz, CDCl_3) δ 171.0, 163.2, 152.4, 142.2, 137.9, 130.0, 126.4, 115.0, 93.9, 68.4, 45.8, 43.7, 43.4, 34.2, 31.2, 26.9, 22.4, 19.3, 13.9, two carbon atoms were not found due to overlapping; IR (film) 2957, 2932, 2872, 1776, 1717, 1593, 1497, 1433, 1348, 1240, 1159, 1092, 1013, 964 cm^{-1} ; HRMS (ESI) Calcd for $\text{C}_{23}\text{H}_{32}\text{O}_7\text{N}_2\text{NaS}^+$ ($[\text{M}+\text{Na}]^+$) 503.1822, Found 503.1816.

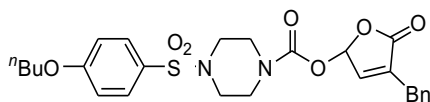


3Me-H-SPL7: ^1H NMR (600 MHz, CDCl_3) δ 7.65 (2H, d, $J = 9.0$ Hz), 7.00 (2H, d, $J = 9.0$ Hz), 6.74 (1H, brs), 5.93 (1H, brs), 4.03 (2H, t, $J = 7.2$ Hz), 3.81 (1H, d, $J = 10.4$ Hz), 3.70 (1H, d, $J = 10.4$ Hz), 3.50-3.39 (2H, m), 3.25 (1H, brs), 3.18 (1H, brs), 2.80 (1H, t, $J = 8.7$ Hz), 2.76 (1H, t, $J = 8.7$ Hz), 2.05 (3H, s), 1.80 (2H, quintet, $J = 7.2$ Hz), 1.51 (2H, sextet, d, $J = 7.2$ Hz), 0.99 (3H, t, $J = 7.8$ Hz); ^{13}C NMR (151 MHz, CDCl_3) δ 169.9, 163.2, 162.7, 152.5, 129.9, 126.3, 119.7, 115.0, 96.1, 68.3, 45.8, 43.6, 43.5, 31.1, 19.3, 13.9, 13.4,

one carbon atom was not found due to overlapping; IR (film) 2961, 2932, 2872, 1792, 1717, 1593, 1435, 1348, 1240, 1159, 1088, 1022, 978 cm^{-1} ; HRMS (ESI) Calcd for $\text{C}_{20}\text{H}_{26}\text{O}_7\text{N}_2\text{NaS}^+$ ($[\text{M}+\text{Na}]^+$) 461.1353, Found 461.1349.

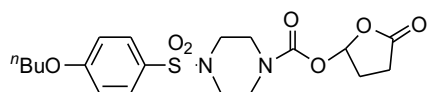


3'Me-SPL7: ^1H NMR (600 MHz, CDCl_3) δ 7.65 (2H, d, $J = 9.0$ Hz), 6.99 (2H, d, $J = 9.0$ Hz), 6.67 (1H, s), 4.03 (2H, t, $J = 6.6$ Hz), 3.82 (1H, d, $J = 12.3$ Hz), 3.70 (1H, d, $J = 12.3$ Hz), 3.44 (1H, t, $J = 10.4$ Hz), 3.40 (1H, t, $J = 10.4$ Hz), 3.25 (1H, d, $J = 9.3$ Hz), 3.18 (1H, d, $J = 9.3$ Hz), 2.78 (1H, t, $J = 9.0$ Hz), 2.73 (1H, t, $J = 9.0$ Hz), 1.93 (3H, s), 1.85 (3H, s), 1.80 (2H, quintet, $J = 6.6$ Hz), 1.51 (2H, sextet, $J = 6.6$ Hz), 0.99 (3H, t, $J = 6.6$ Hz); ^{13}C NMR (151 MHz, CDCl_3) δ 171.7, 163.2, 153.3, 152.8, 129.9, 127.4, 126.4, 115.0, 95.4, 68.4, 45.8, 43.7, 43.5, 31.2, 19.3, 13.9, 11.5, 8.7, one carbon atom was not found due to overlapping; IR (film) 2959, 2928, 2872, 1775, 1722, 1595, 1435, 1348, 1310, 1240, 1161, 1123, 1084, 989 cm^{-1} ; HRMS (ESI) Calcd for $\text{C}_{21}\text{H}_{28}\text{O}_7\text{N}_2\text{NaS}^+$ ($[\text{M}+\text{Na}]^+$) 475.1509, Found 475.1506.

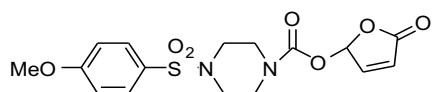


Bn-SPL7: ^1H NMR (600 MHz, CDCl_3) δ 7.64 (2H, d, $J = 8.7$ Hz), 7.34 (2H, t, $J = 7.2$ Hz), 7.27 (1H, d, $J = 7.2$ Hz), 7.22 (2H, d, $J = 7.2$ Hz), 6.98 (2H, d, $J = 8.7$ Hz), 6.82 (1H, s), 6.62 (1H, d, $J = 1.2$ Hz), 4.02 (2H, t, $J = 7.2$ Hz), 3.73 (1H, d, $J = 12.6$ Hz), 3.66-3.57 (3H,

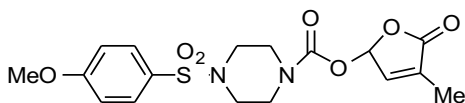
m), 3.46 (1H, t, $J = 10.2$ Hz), 3.41 (1H, t, $J = 10.2$ Hz), 3.15 (1H, brs), 3.09 (1H, brs), 2.83 (1H, t, $J = 8.2$ Hz), 2.79 (1H, t, $J = 8.2$ Hz), 1.80 (2H, quintet, $J = 7.2$ Hz), 1.51 (2H, sextet, $J = 7.2$ Hz), 0.99 (3H, t, $J = 7.2$ Hz); ^{13}C NMR (151 MHz, CDCl_3) δ 170.3, 163.2, 152.3, 142.5, 139.0, 136.3, 129.9, 129.1, 129.0, 127.3, 126.4, 115.0, 94.1, 68.4, 45.8₂, 45.7₇, 43.6, 43.4, 31.9, 31.2, 19.3, 13.9; IR (film) 2959, 2932, 2872, 1778, 1717, 1595, 1497, 1435, 1348, 1240, 1161, 1092, 1015, 962 cm^{-1} ; HRMS (ESI) Calcd for $\text{C}_{26}\text{H}_{30}\text{O}_7\text{N}_2\text{NaS}^+$ ($[\text{M}+\text{Na}]^+$) 537.1666, Found 537.1662.



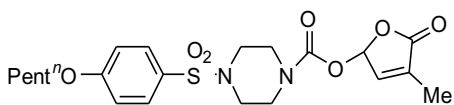
sat-H-SPL7: ^1H NMR (600 MHz, CDCl_3) δ 7.66 (2H, d, $J = 8.7$ Hz), 6.99 (2H, d, $J = 8.7$ Hz), 6.57 (1H, d, $J = 5.4$ Hz), 4.03 (2H, t, $J = 7.2$ Hz), 3.72 (1H, d, $J = 10.2$ Hz), 3.64 (1H, d, $J = 10.2$ Hz), 3.47 (2H, br), 3.15 (1H, br), 3.11 (1H, br), 2.83 (2H, br), 2.68-2.62 (1H, m), 2.55-2.46 (2H, m), 2.26-2.20 (1H, m), 1.80 (2H, quintet, $J = 7.2$ Hz), 1.51 (2H, sextet, $J = 7.2$ Hz), 1.00 (3H, t, $J = 7.2$ Hz); ^{13}C NMR (151 MHz, CDCl_3) δ 175.4, 163.2, 152.4, 130.0, 126.4, 115.0, 96.8, 68.4, 45.8, 43.6, 43.2, 31.2, 28.0, 26.1, 19.3, 13.9, one carbon atom was not found probably due to overlapping; IR (film) 2959, 2932, 2871, 1792, 1710, 1594, 1498, 1436, 1346, 1245, 1158, 1123, 1048, 951, 927 cm^{-1} ; HRMS (ESI) Calcd for $\text{C}_{19}\text{H}_{26}\text{O}_7\text{N}_2\text{NaS}^+$ ($[\text{M}+\text{Na}]^+$) 449.1353, Found 449.1346.



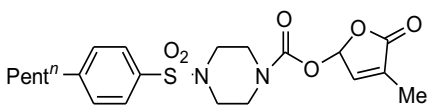
pMeO-H-SPL7: ^1H NMR (600 MHz, CDCl_3) δ 7.68 (2H, dt, $J = 9.0, 2.4$ Hz), 7.27 (1H, dd, $J = 7.2, 1.8$ Hz), 7.02 (2H, dt, $J = 9.0, 2.4$ Hz), 6.96 (1H, t, $J = 1.8$ Hz), 6.29 (1H, d, $J = 7.2$ Hz), 3.89 (3H, s), 3.77 (1H, d, $J = 12.6$ Hz), 3.67 (1H, d, $J = 12.6$ Hz), 3.49 (1H, t, $J = 11.0$ Hz), 3.45 (1H, t, $J = 11.0$ Hz), 3.20 (1H, br), 3.14 (1H, br), 2.85 (1H, t, $J = 11.0$ Hz), 2.81 (1H, t, $J = 11.0$ Hz); ^{13}C NMR (151 MHz, CDCl_3) δ 169.7, 163.6, 152.2, 149.7, 130.0, 126.8, 125.5, 114.7, 95.4, 55.8, 45.8, 43.7, 43.5, one carbon atom was not found due to overlapping; IR (film) 2982, 2847, 1792, 1719, 1595, 1499, 1437, 1348, 1242, 1161, 1092, 1018, 926 cm^{-1} ; HRMS (ESI) Calcd for $\text{C}_{16}\text{H}_{18}\text{O}_7\text{N}_2\text{NaS}^+$ ($[\text{M}+\text{Na}]^+$) 405.0727, Found 405.0721.



pMeO-SPL7: ^1H NMR (600 MHz, CDCl_3) δ 7.67 (2H, d, $J = 8.4$ Hz), 7.01 (2H, d, $J = 8.4$ Hz), 6.85-6.84 (1H, m), 6.83 (1H, brs), 3.89 (3H, s), 3.77 (1H, brd, $J = 12.2$ Hz), 3.66 (1H, brd, $J = 12.2$ Hz), 3.52-3.40 (2H, m), 3.19 (1H, brs), 3.13 (1H, brs), 2.84 (1H, t, $J = 8.4$ Hz), 2.79 (1H, t, $J = 8.4$ Hz), 1.97 (3H, s); ^{13}C NMR (151 MHz, CDCl_3) δ 171.1, 163.4, 152.3, 142.1, 134.4, 129.8, 126.6, 114.5, 93.7, 55.7, 45.7, 43.5, 43.3, 10.6, one carbon atom was not found due to overlapping; IR (film) 2895, 2855, 1780, 1717, 1595, 1435, 1346, 1242, 1192, 1061, 1016, 955 cm^{-1} ; HRMS (ESI) Calcd for $\text{C}_{17}\text{H}_{20}\text{O}_7\text{N}_2\text{NaS}^+$ ($[\text{M}+\text{Na}]^+$) 419.0883, Found 419.0871.



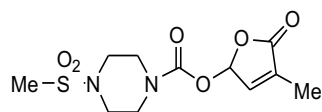
pPentO-SPL7: ^1H NMR (600 MHz, CDCl_3) δ 7.65 (2H, d, $J = 8.4$ Hz), 6.99 (2H, d, $J = 8.4$ Hz), 6.85 (1H, brs), 6.82 (1H, brs), 4.02 (2H, t, $J = 7.0$ Hz), 3.76 (1H, d, $J = 12.6$ Hz), 3.66 (1H, d, $J = 12.6$ Hz), 3.48 (1H, t, $J = 9.0$ Hz), 3.44 (1H, t, $J = 9.0$ Hz), 3.18 (1H, br), 3.12 (1H, br), 2.84 (1H, t, $J = 9.0$ Hz), 2.79 (1H, t, $J = 9.0$ Hz), 1.96 (3H, s), 1.82 (2H, quintet, $J = 7.0$ Hz), 1.45 (2H, quintet, $J = 7.0$ Hz), 1.40 (2H, sextet, $J = 7.0$ Hz), 0.94 (3H, t, $J = 7.0$ Hz); ^{13}C NMR (151 MHz, CDCl_3) δ 171.2, 163.2, 152.4, 142.1, 134.6, 129.9, 126.4, 115.0, 93.8, 68.7, 45.8, 43.6, 43.4, 28.8, 28.2, 22.5, 14.1, 10.7, one carbon atom was not found due to overlapping; IR (film) 2936, 2922, 1769, 1722, 1595, 1433, 1348, 1242, 1165, 1092, 1015, 957 cm^{-1} ; HRMS (ESI) Calcd for $\text{C}_{21}\text{H}_{28}\text{O}_7\text{N}_2\text{NaS}^+$ ($[\text{M}+\text{Na}]^+$) 475.1509, Found 475.1507.



pPent-SPL7: ^1H NMR (600 MHz, CDCl_3) δ 7.63 (2H, d, $J = 8.4$ Hz), 7.35 (2H, d, $J = 8.4$ Hz), 6.84 (1H, brs), 6.83 (1H, s), 3.77 (1H, d, $J = 12.3$ Hz), 3.67 (1H, d, $J = 12.3$ Hz), 3.48 (1H, t, $J = 9.6$ Hz), 3.44 (1H, t, $J = 9.6$ Hz), 3.21 (1H, t, $J = 6.0$ Hz), 3.15 (1H, t, $J = 6.0$ Hz), 2.86 (1H, t, $J = 8.4$ Hz), 2.81 (1H, t, $J = 8.4$ Hz), 2.68 (2H, t, $J = 7.2$ Hz), 1.96 (3H, s), 1.65 (2H, quintet, $J = 7.2$ Hz), 1.39-1.30 (4H, m), 0.91 (3H, t, $J = 7.2$ Hz); ^{13}C NMR (151 MHz, CDCl_3) δ 171.1, 152.4, 149.3, 142.1, 134.7, 132.5, 129.4, 127.9, 93.9, 45.8, 43.7, 43.5, 36.0, 31.6, 30.8, 22.6, 10.8, one carbon atom was not found due to overlapping; IR

(film) 2928, 2857, 1780, 1721, 1435, 1350, 1242, 1167, 1126, 1092, 1015, 955 cm^{-1} ;

HRMS (ESI) Calcd for $\text{C}_{21}\text{H}_{28}\text{O}_6\text{N}_2\text{NaS}^+$ ($[\text{M}+\text{Na}]^+$) 459.1560, Found 459.1558.



Ms-SPL7: ^1H NMR (600 MHz, acetone- d_6) δ 7.19 (1H, q, $J = 1.5$ Hz), 6.89 (1H, s), 3.67

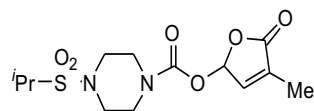
(2H, br), 3.63-3.45 (3H, m), 3.33-3.15 (3H, m), 2.86 (3H, s), 1.93 (3H, d, $J = 1.5$ Hz); ^{13}C

NMR (151 MHz, acetone- d_6) δ 171.9, 153.3, 144.1, 134.4, 94.7, 46.1, 44.6, 44.3, 34.6,

10.5, one carbon atom was not found probably due to overlapping; IR (film) 2933, 2854,

1776, 1716, 1437, 1340, 1324, 1284, 1241, 1206, 1153, 1096, 1064, 1047, 1012, 957, 945

cm^{-1} ; HRMS (ESI) Calcd for $\text{C}_{11}\text{H}_{16}\text{O}_6\text{N}_2\text{NaS}^+$ ($[\text{M}+\text{Na}]^+$) 327.0621, Found 327.0616.



iPrSO₂-SPL7: ^1H NMR (600 MHz, acetone- d_6) δ 7.19 (1H, br), 6.88 (1H, s), 3.59 (2H, br),

3.51 (2H, br), 3.44-3.32 (4H, m), 3.31 (1H, septet, $J = 6.6$ Hz), 1.93 (3H, s), 1.29 (6H, d, J

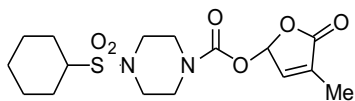
$= 6.6$ Hz); ^{13}C NMR (151 MHz, acetone- d_6) δ 171.9, 153.4, 144.1, 134.4, 94.7, 53.5, 46.5,

45.4, 45.1, 17.0, 10.5, one carbon atom was not found probably due to overlapping; IR

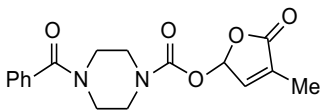
(film) 2985, 2927, 2863, 1772, 1716, 1432, 1319, 1282, 1240, 1206, 1142, 1095, 1014,

984, 954 cm^{-1} ; HRMS (ESI) Calcd for $\text{C}_{13}\text{H}_{20}\text{O}_6\text{N}_2\text{NaS}^+$ ($[\text{M}+\text{Na}]^+$) 355.0934, Found

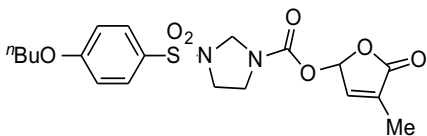
355.0932.



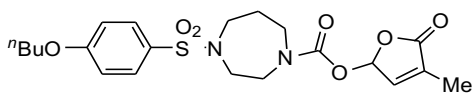
HexSO₂-SPL7: ¹H NMR (600 MHz, CDCl₃) δ 6.90 (2H, br), 3.72 (1H, d, *J* = 10.2 Hz), 3.61 (1H, d, *J* = 10.2 Hz), 3.52-3.37 (4H, m), 3.35-3.24 (2H, m), 2.91 (1H, tt, *J* = 13.2, 3.6 Hz), 2.10 (2H, d, *J* = 13.2 Hz), 1.99 (3H, s), 1.89 (2H, d, *J* = 13.2 Hz), 1.71 (1H, d, *J* = 13.2 Hz), 1.50 (2H, qd, *J* = 13.2, 3.0 Hz), 1.27 (1H, qt, *J* = 13.2, 3.0 Hz), 1.90 (1H, qt, *J* = 13.2, 3.0 Hz); ¹³C NMR (151 MHz, CDCl₃) δ 171.2, 152.7, 142.2, 134.7, 93.9, 61.9, 46.0, 44.9, 44.6, 26.7, 25.3, 25.2, 10.8, one carbon atom was not found probably due to overlapping; IR (film) 2933, 2860, 1772, 1716, 1429, 1319, 1282, 1240, 1206, 1144, 1094, 1014, 984, 951 cm⁻¹; HRMS (ESI) Calcd for C₁₆H₂₄O₆N₂NaS⁺ ([M+Na]⁺) 395.1247, Found 395.1244.



Bz-SPL7: ¹H NMR (600 MHz, CDCl₃) δ 7.47-7.39 (5H, m), 6.91 (2H, br), 4.00-3.30 (8H, m), 1.99 (3H, s); ¹³C NMR (151 MHz, CDCl₃) δ 171.2, 170.8, 152.8, 142.1, 135.2, 134.7, 130.3, 128.8, 127.2, 94.0, 47.2, 44.3, 42.0, 10.8, one carbon atom was not found probably due to overlapping; IR (film) 2929, 2864, 1773, 1717, 1635, 1461, 1429, 1242, 1230, 1008, 959 cm⁻¹; HRMS (ESI) Calcd for C₁₇H₁₈O₅N₂Na⁺ ([M+Na]⁺) 353.1108, Found 353.1103.



Im-SPL7: ^1H NMR (600 MHz, CDCl_3) *rotamer A* δ 7.73 (2H, d, $J = 9.0$ Hz), 7.02 (2H, d, $J = 9.0$ Hz), 6.88 (1H, s), 6.81 (1H, s), 4.68 (1H, d, $J = 9.0$ Hz), 4.62 (1H, d, $J = 9.0$ Hz), 4.09-4.01 (2H, m), 3.57 (1H, dt, $J = 12.0, 6.0$ Hz), 3.53-3.48 (1H, m), 3.32 (1H, dt, $J = 9.6, 6.6$ Hz), 3.26-3.18 (1H, m), 2.02 (3H, s), 1.84-1.77 (2H, m), 1.51 (2H, sextet, $J = 7.8$ Hz), 0.99 (3H, t, $J = 7.8$ Hz); *rotamer B* δ 7.76 (2H, d, $J = 9.0$ Hz), 7.00 (2H, d, $J = 9.0$ Hz), 6.81 (1H, s), 6.79 (1H, s), 4.72 (2H, s), 4.09-4.01 (2H, m), 3.60 (1H, dt, $J = 12.0, 6.0$ Hz), 3.53-3.48 (1H, m), 3.26-3.18 (2H, m), 1.96 (3H, s), 1.84-1.77 (2H, m), 1.51 (2H, sextet, $J = 7.8$ Hz), 0.99 (3H, t, $J = 7.8$ Hz); ^{13}C NMR (151 MHz, CDCl_3) *mixture of rotamers* δ 171.1, 171.0, 163.6₃, 163.5₈, 150.9, 150.6, 141.8₉, 141.8₆, 134.9, 134.7, 130.0, 129.8, 127.2₃, 127.1₈, 115.4, 115.2, 93.5, 68.5₁, 68.4₈, 62.5, 61.9, 47.2, 46.4, 44.2, 44.0, 31.1, 19.3, 13.9, 10.8, 10.7; IR (film) 2959, 2874, 1778, 1726, 1593, 1422, 1348, 1260, 1157, 1092, 959 cm^{-1} ; HRMS (ESI) Calcd for $\text{C}_{19}\text{H}_{24}\text{O}_7\text{N}_2\text{NaS}^+$ ($[\text{M}+\text{Na}]^+$) 447.1196, Found 447.1191.



Diazepine-SPL7: ^1H NMR (600 MHz, CDCl_3) *mixture of rotamers* δ 7.71-7.66 (2+2H, m), 6.97 (2+2H, d, $J = 8.4$ Hz), 6.89 (1H, q, $J = 1.2$ Hz), 6.88 (1H, q, $J = 1.2$ Hz), 6.87 (1H, s), 6.86 (1H, s), 4.02 (2+2H, t, $J = 6.8$ Hz), 3.74-3.67 (1H, m), 3.65-3.39 (5+6H, m), 3.18 (1H, ddd, $J = 13.8, 7.8, 3.6$ Hz), 3.12-3.01 (1+2H, m), 2.01-1.93 (4+4H, m), 1.93-1.86 (1+1H, m), 1.79 (2+2H, quintet, $J = 6.6$ Hz), 1.50 (2+2H, sextet, $J = 6.8$ Hz), 0.98 (3+3H, t, $J = 6.8$ Hz); ^{13}C NMR (151 MHz, CDCl_3) *mixture of rotamers* δ 171.3₂, 171.2₉, 162.7, 153.6, 153.2, 142.4, 142.3, 134.5, 134.4, 130.4₀, 130.3₇, 129.0₇, 129.0₅, 114.9, 93.8, 68.3, 49.8,

49.7, 48.9, 47.8, 47.7, 46.5, 46.0, 31.2, 28.3, 27.8, 19.3, 13.9, 10.7; IR (film) 2957, 2872, 1780, 1721, 1713, 1595, 1423, 1331, 1256, 1153, 1092, 1013, 959 cm⁻¹; HRMS (ESI) Calcd for C₂₁H₂₈O₇N₂NaS⁺ ([M+Na]⁺) 475.1509, Found 475.1510.

Identification of the byproduct of SAM molecules

During the structure–activity relationship (SAR) study, we found that some of SAM compounds exhibited markedly decreased germination activity after gel permeation chromatography (GPC) purification. For example, while silica gel column-purified SAM8 possessing a 4-MeOC₆H₄SO₂ moiety showed moderate activity (μM level), the GPC-purified one did not induce any germination of *Striga* seeds, despite of nearly identical purities of the two samples in ¹H NMR analysis (Fig. S3A). We anticipated that SAM8 was contaminated with a very small amount of an extremely active impurity and decided to pursue isolation of the impurity with the aim of determining its structure. *N*-Furyl carbonyl piperazine (2.3 g, 13.0 mmol) was treated with 4-MeOC₆H₄SO₂Cl (2.8 g, 13.7 mmol) and triethylamine (2.7 mL, 19.5 mmol) in CH₂Cl₂ (130 mL) for 19 h at room temperature (see above for the detailed procedure). The reaction mixture was quenched upon addition of a saturated aqueous solution of NaHCO₃ and the aqueous phase was extracted with ethyl acetate twice. The combined organic extracts were dried over Na₂SO₄, filtered, and concentrated to afford a crude mixture which was subjected to fractional silica gel column chromatography (ethyl acetate/hexane = 1:1 as eluent) to remove most of SAM8 (Fig. S3B). The remainder was combined and concentrated under reduced pressure to form a residual sample that indeed exhibited moderate germination activity. The residue was re-

1 subjected to silica gel column chromatography (ethyl acetate/hexane = 3:1 to ethyl acetate
2 as eluent) and divided into eight fractions. A subsequent germination assay of each
3 fractions indicated that fractions #2 and #3 stimulated germination. A combined sample of
4 these two fractions was concentrated in vacuo to obtain 0.6 mg of the residue, which was
5 analyzed using liquid chromatography–mass spectrometry (LC-MS; Fig. S3C). The
6 analysis revealed that the sample contained several unidentified compounds and SAM8 as
7 major components and thus the germination activity of all the detected compounds was
8 evaluated. Compound X (m/z 382), which showed a peak at 10.2 min, exhibited the highest
9 germination activity, but the quantity of X isolated through preparative HPLC was
10 insufficient for reliable ^1H and ^{13}C NMR analysis for precise structural determination (Fig.
11 S3D). Considering the difference in m/z units between X and SAM8 (m/z 350), we
12 hypothesized that X may be formed through oxidative degradation of SAM8, and promptly
13 treated SAM8 with various oxidants. Eventually, treatment of SAM8 (262.8 mg, 0.75
14 mmol) with singlet oxygen under dye-sensitized photo-irradiative conditions (methylene
15 blue, 3.0 mg) in MeOH (7.5 mL) at room temperature for 27 h gave a compound (2.6%
16 yield), analytically identical to X based on HPLC, MS, and NMR analysis. Careful
17 spectroscopic analysis allowed us to determine its structure, as shown in Fig. S3A, where
18 the furyl carbonyl moiety in SAM8 was converted into a butenolide structure similar to the
19 D-ring subunit of SLs. The structure of X as an oxygenated SAM8 was finally confirmed
20 through straightforward synthesis from piperazine (see above for detailed procedure). One
21 of the two nitrogen atoms of piperazine (459.4 mg, 0.8 mmol) was selectively sulfonylated
22 by reacting with 4-MeOC₆H₄SO₂Cl (41.3 mg, 0.2 mmol) and triethylamine (0.042 mL, 0.3

mmol) in CH₂Cl₂ (2.0 mL) at room temperature. The remaining nitrogen atom was converted into carbamoyl chloride by treatment with triphosgene (30.0 mg, 0.1 mmol) in the presence of triethylamine (0.042 mL, 0.3 mmol) in CH₂Cl₂ (0.38 mL) at 0 °C. The desired oxygenated SAM8 (pMeO-H-SPL7) was obtained in 55% yield from the reaction between the carbamoyl chloride and 5-hydroxyfuran-2(5*H*)-one (30.0 mg, 0.3 mmol) with triethylamine (0.042 mL, 0.3 mmol) and *N,N*-dimethyl-4-aminopyridine (DMAP, 10 mol%) in CH₂Cl₂ (1.0 mL) at room temperature. Its derivative, oxygenated SAM690 (H-SPL7) with the 4-ⁿBuOC₆H₄SO₂ moiety, was prepared following the same procedure and used for biological studies described in the main text.

Figure S1

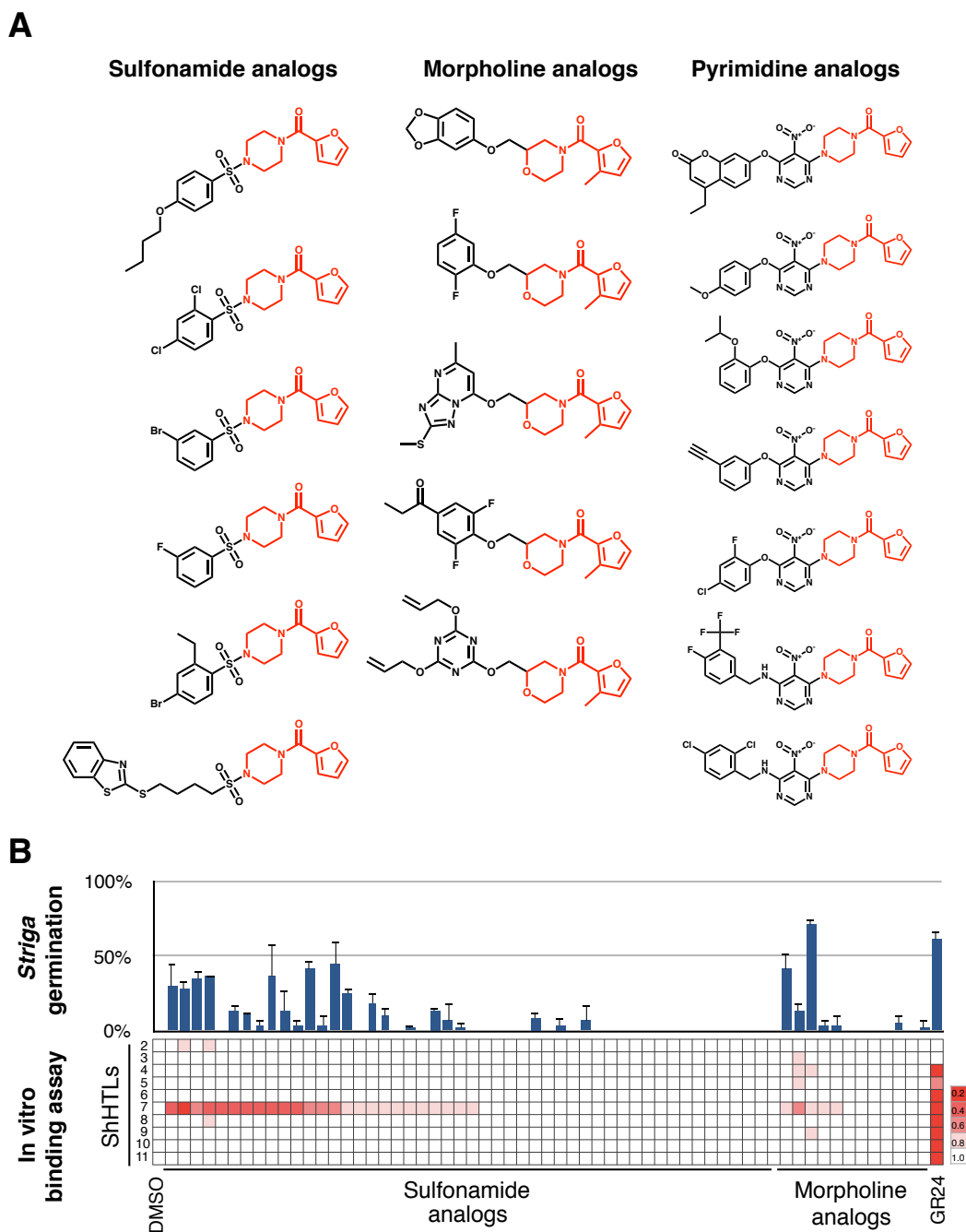


Fig. S1. Structures of germination stimulants for *Striga* identified through chemical screening. (A) Initial hits from chemical screening. Furan connected to six-membered heterocycles through a carbonyl group was common to all the structures as indicated by red. Based on extended structures, these stimulants were grouped into sulfonamide, morpholine or pyrimidine analogs. **(B)** Relationship between *Striga* germination and in vitro binding to ShHTL proteins in

newly synthesized analogs. The top panel indicates *Striga* germination with 10 μ M of analogs. Error bar indicates s.d. ($n = 3$ biological replicates). The bottom panel represents bindings indicated by YLG competition assay with 10 μ M of compounds. Average of technical replicates was presented as a heat map ($n = 2$). Structures and numeric data for synthesized analogs in (B) are presented in table S1.

Figure S2

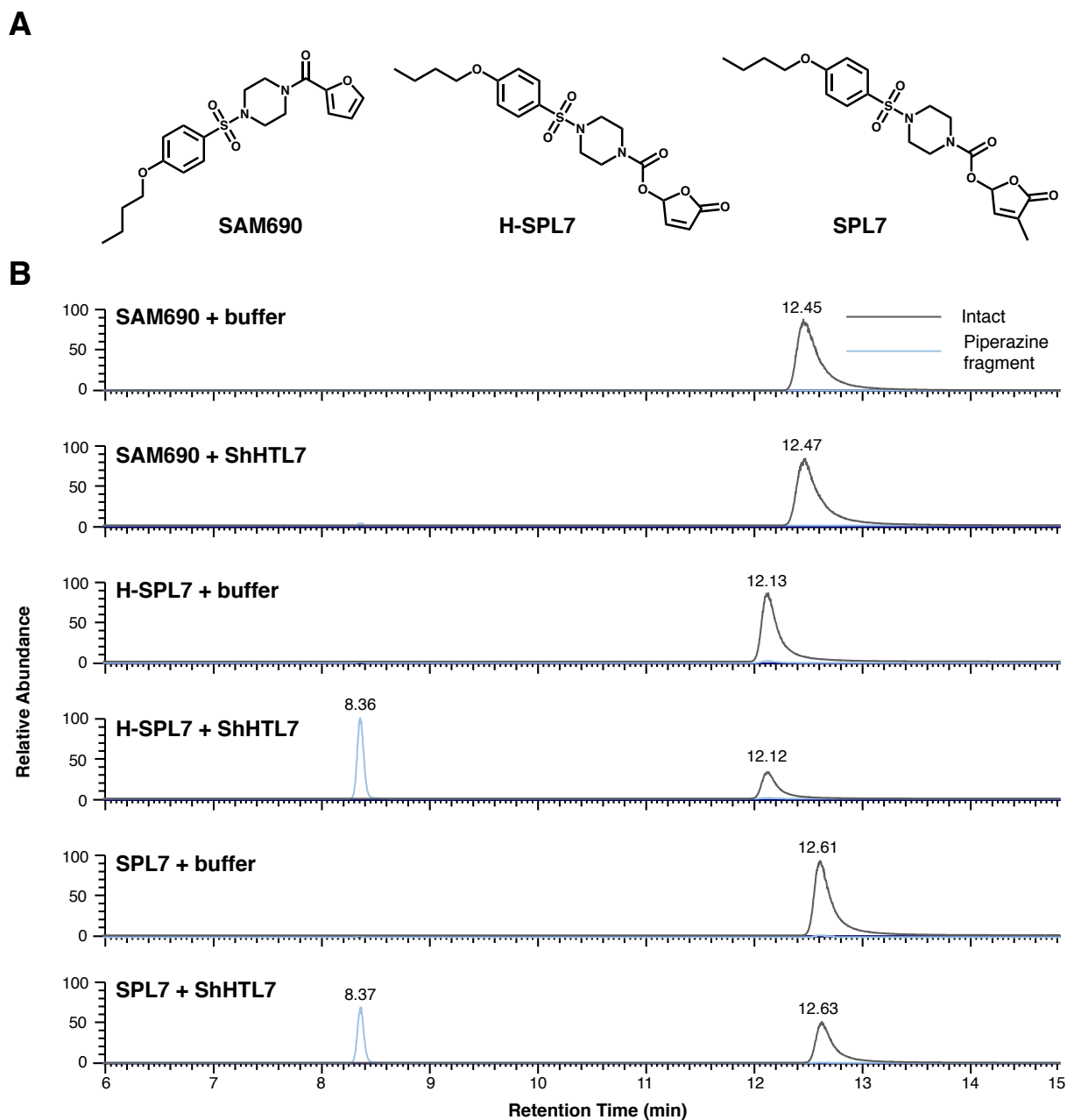


Fig. S2. Hydrolysis of SPL7 by ShHTL7. (A) Structures of SAM690 and SPL7 molecules. (B) LC chromatogram after reaction with ShHTL7. The grey line presents an extracted ion chromatogram corresponding to m/z at 393.1459–393.1499 for SAM690, 425.1356–425.1398 for H-SPL7 and 439.1511–439.1555 for SPL7. The blue

chromatogram presents alkyldisulfonylpiperazine fragment in m/z at 299.1409–299.14390 as a result of hydrolysis. 1 μM of small molecules were reacted with 0.6 μM of the recombinant ShHTL7 protein for 30 min. Equivalent amount of buffer was added for control experiments.

Figure S3

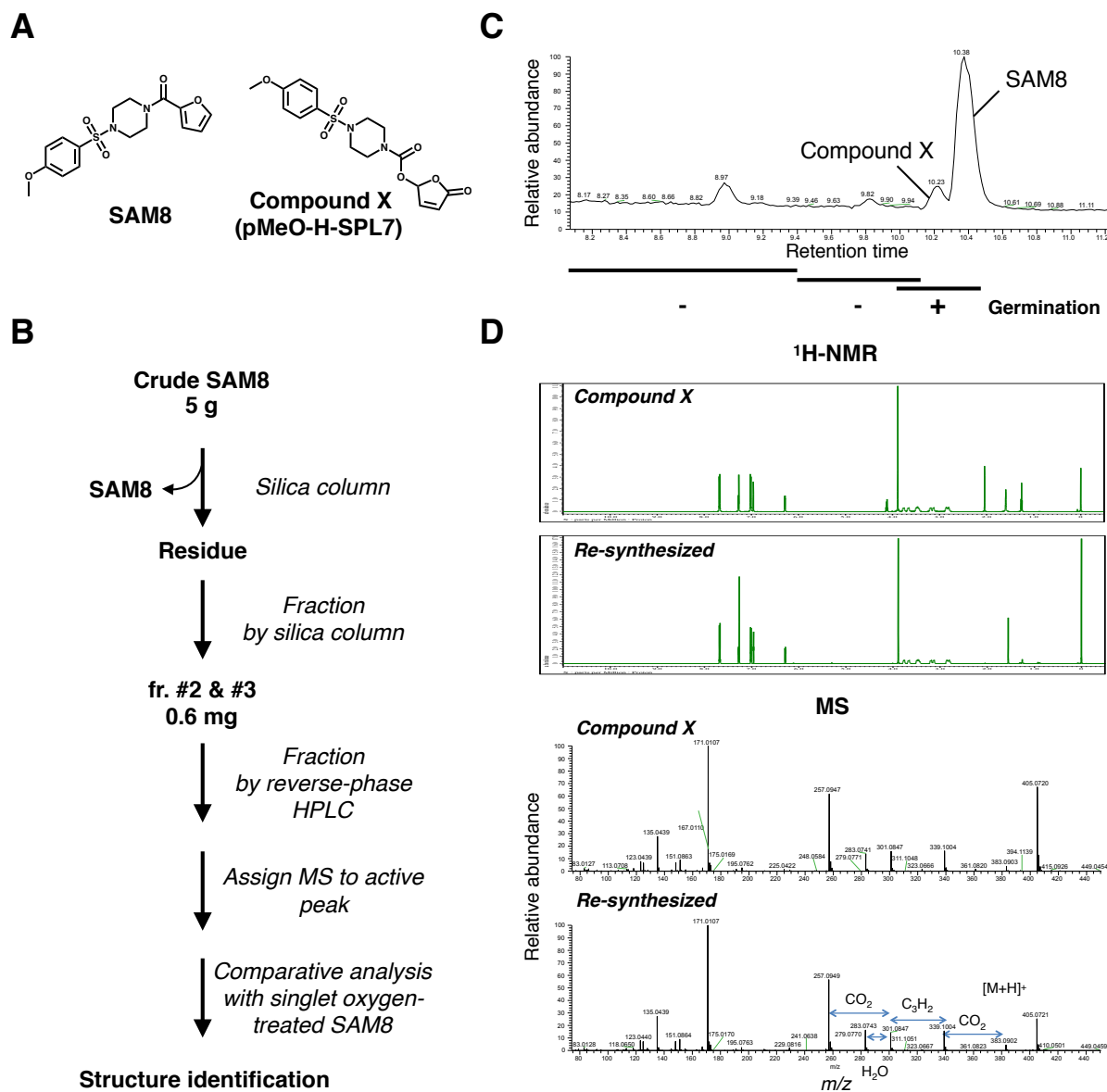


Fig. S3. Identification of synthetic by-product of SAM8
(A) Structure of SAM8 and pMeO-H-SPL7. **(B)** Scheme for identification of compound X. **(C)** Reverse-phase HPLC chromatogram shown with bioassay for *Striga* germination.

(D) ¹H NMR chart and mass spectrum for compound X and re-synthesized pMeO-H-SPL7. Additional information is provided in the supplementary methods.

Figure S4

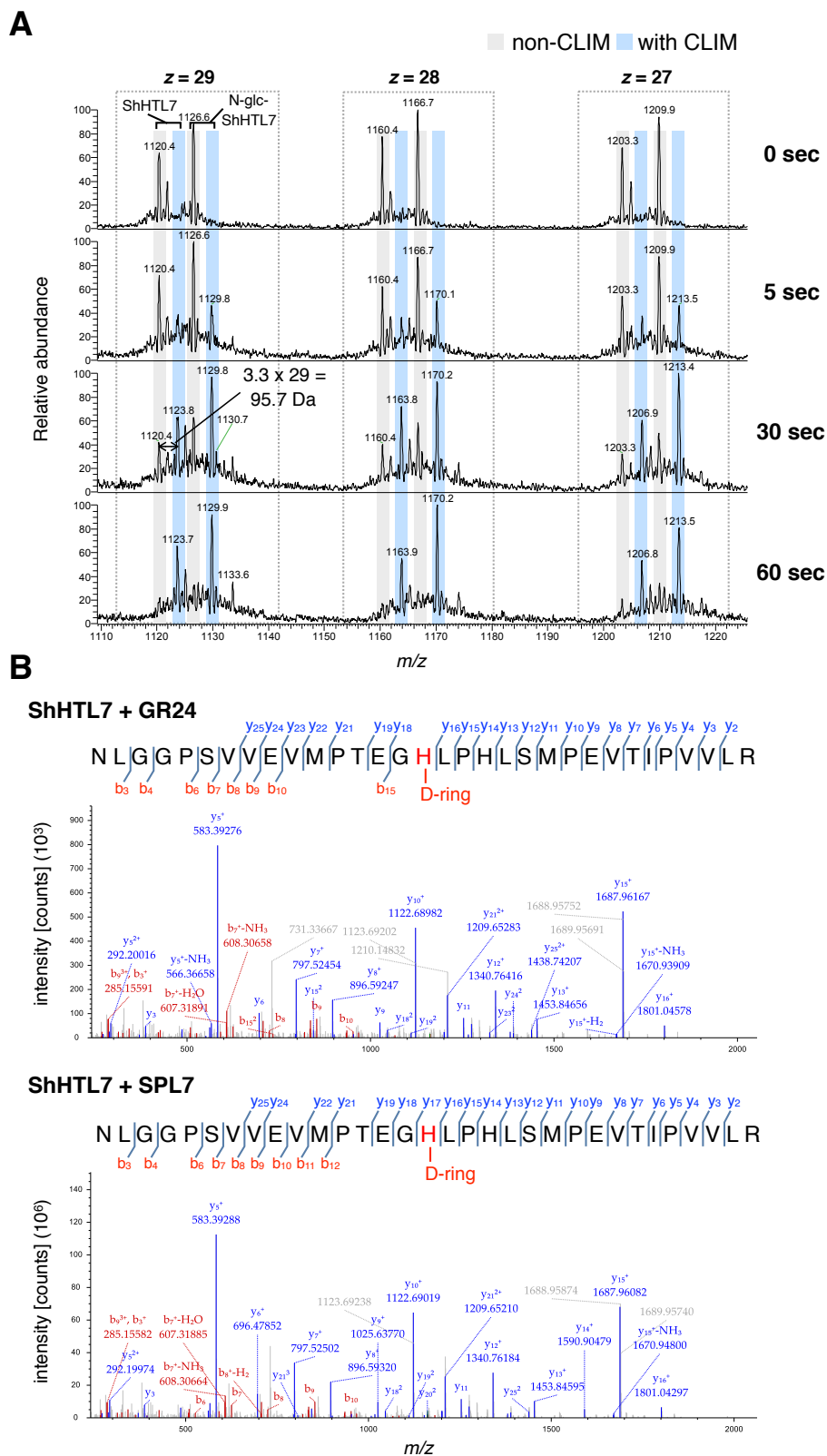
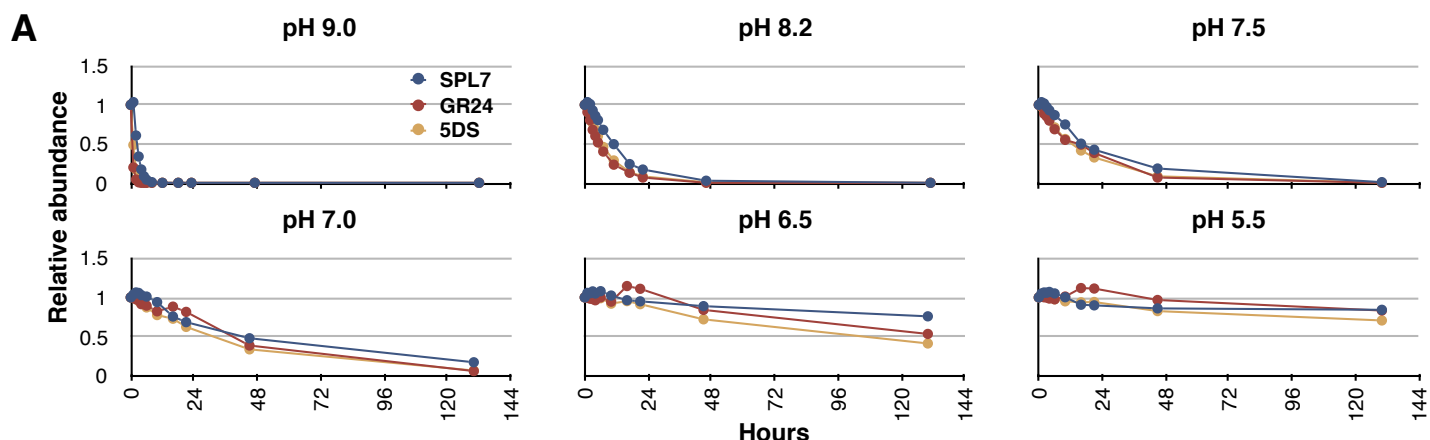


Fig. S4. Detection of CLIM on the histidine residue of the catalytic triad on ShHTL7. (A) Mass spectrum of ShHTL7 protein reacted with SPL7. A reaction with SPL7 shifts the peak by m/z 96 corresponding to substitution of a proton ($H = 1.0000$ Da) with D-ring ($C_5H_5O_2 = 97.0284$ Da). D-ring adduct is also observed in alpha-*N*-gluconoylated ShHTL7. From left, $z = 29$, 28 and 27 . **(B)** Detection of D-ring adduct at histidine 246 residue in ShHTL7. MS/MS spectra of a

quadruply charged peptide (231-NLGGPSVVEVMPTEGHLPHLSMPEVTIPVVL R-262) of ShHTL7 at m/z 875.9340 corresponding to the mass of the $C_5H_4O_2$ modification of H246. The reaction mixture of ShHTL7 with (+)-GR24 or SPL7 was digested by trypsin before MS/MS analysis. Labelled peak corresponds to mass of y and b ions of the modified peptide. The D-ring adduct was not detected in DMSO control.

Figure S5



B

Dose (mg/kg)	Number of samples (female rat)	Clinical sign	Body weight (8 days)	Necropsy
5	5	No abnormal signs	No abnormal change	No abnormal change
50	5	No abnormal signs	No abnormal change	No abnormal change
300	5	No abnormal signs	No abnormal change	No abnormal change

C

S9 mix	Test material dose (µg/plate)	Number of revertants (number of colonies / plate)		
		Base-pair substitution type		Frame-shift type
		TA100	WP2 <i>uvrA</i>	TA98
With S9 mix	Negative control	93	22	23
		84	23	24
	4.9	88	34	26
		79	24	28
	19.5	89	23	18
		80	34	28
	78.1	104	23	25
		101	30	30
	312.5*	84	22	21
		83	26	22
	1250*	99	18	30
		96	25	28
	5000*	95	26	22
		95	26	22
Without S9 mix	Negative control	96	24	38
		116	37	34
	4.9	95	24	36
		119	21	30
	19.5	148	24	33
		115	34	40
	78.1	138	28	34
		107	37	32
	312.5	120	27	33
		108	36	39
	1250*	91	32	33
		106	27	34
	5000*	109	21	32
		109	21	32
Positive control not requiring S9 mix	Name	AF-2	AF-2	AF-2
	Dose (µg/plate)	0.01	0.01	0.1
	number of colonies/plate	824	265	649
Positive control requiring S9 mix	Name	2-AA	2-AA	2-AA
	Dose (µg/plate)	1	10	0.5
	number of colonies/plate	1843	877	780
		1866	947	751
		1866	947	751

Fig. S5. Stability and toxicology of SPL7 (A) Stability of SPL7 at various pH conditions. Similar to 5DS or GR24, SPL7 is not stable at high pH range. **(B)** Acute toxicity test of SPL7. Single oral administration of SPL7 to female rats did not cause detectable change in clinical sign, body weight, and necropsy within 14 days. The analysis suggests that the lethal dose of SPL7 for the rat is >300 mg/kg. **(C)** Ames test of SPL7. TA100: *Salmonella typhimurium* strain TA100, WP2 *uvrA*: *Escherichia coli* WPA2 *uvrA*, TA98: *Salmonella typhimurium* strain TA98, AF-2: 2-(furyl)-3-(5-nitro-2-furyl)acrylamide, and 2-AA: 2-aminoanthracene. Asterisk indicates observing precipitation. Mutagenicity assays (Ames tests) using *Salmonella typhimurium* and *Escherichia coli* were negative for SPL7. The analyses were outsourced to an analysis company.

Figure S6

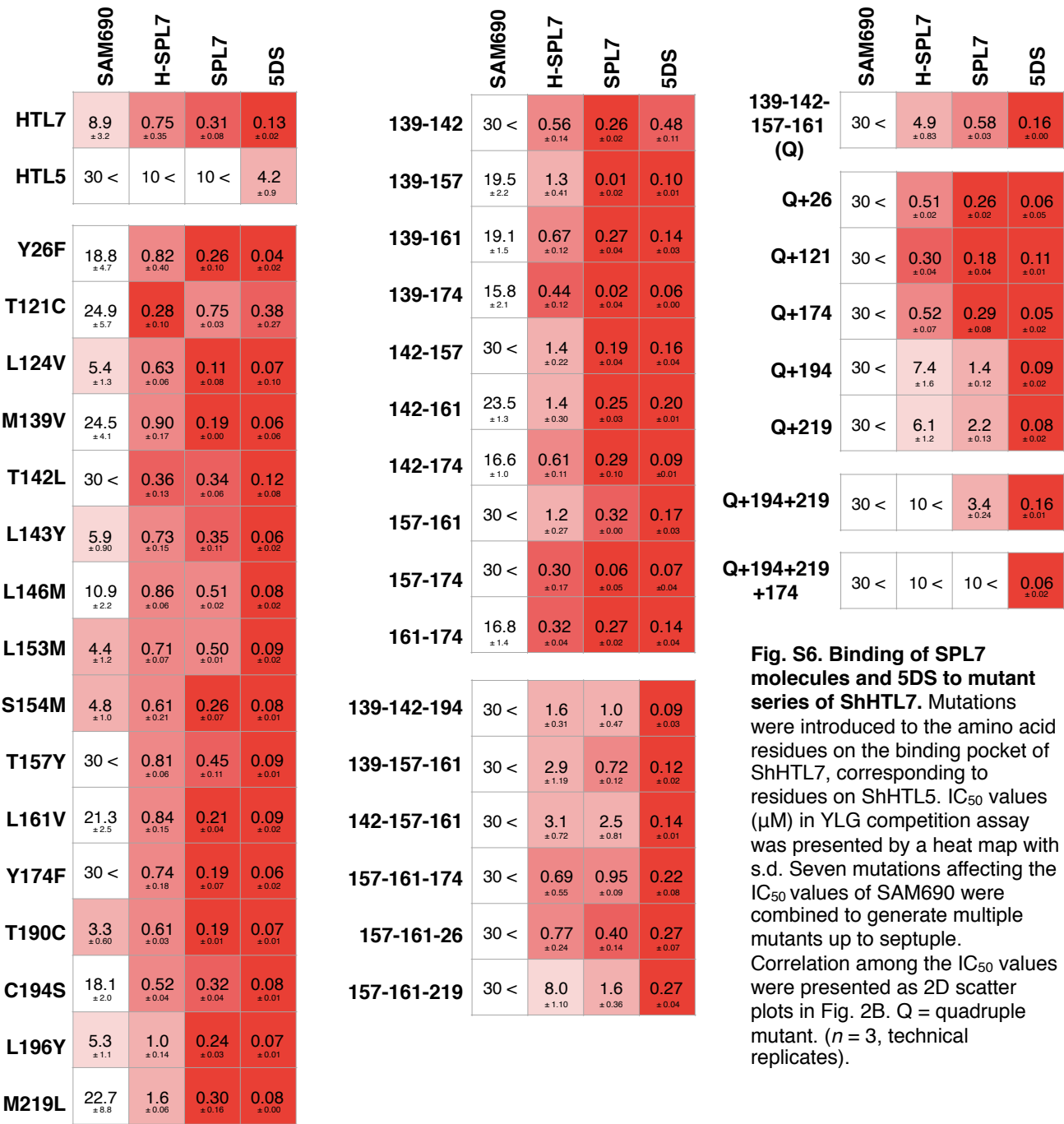


Fig. S6. Binding of SPL7 molecules and 5DS to mutant series of ShHTL7. Mutations were introduced to the amino acid residues on the binding pocket of ShHTL7, corresponding to residues on ShHTL5. IC₅₀ values (μM) in YLG competition assay was presented by a heat map with s.d. Seven mutations affecting the IC₅₀ values of SAM690 were combined to generate multiple mutants up to septuple. Correlation among the IC₅₀ values were presented as 2D scatter plots in Fig. 2B. Q = quadruple mutant. (n = 3, technical replicates).

Figure S7

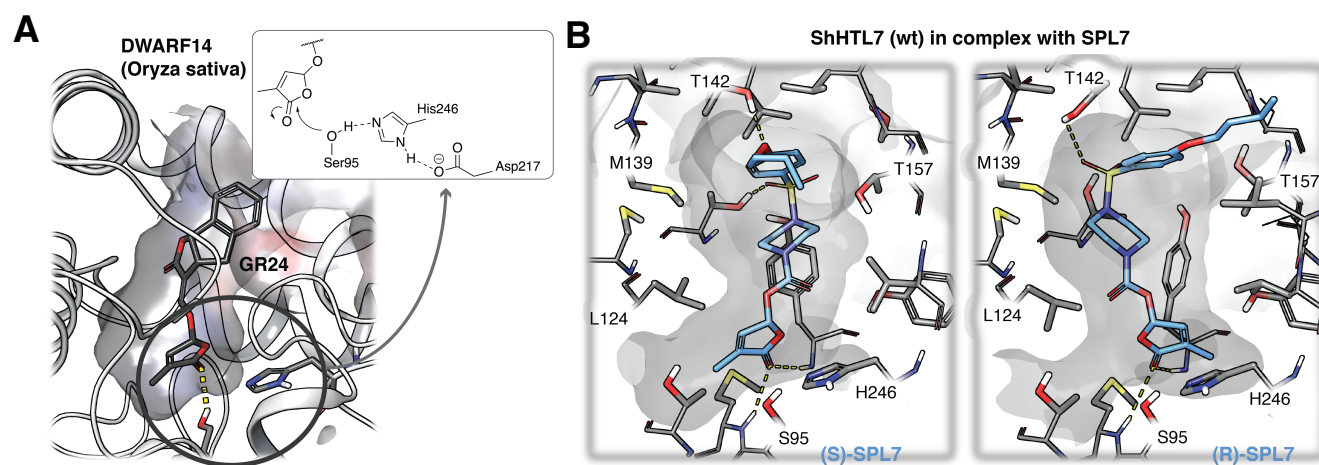
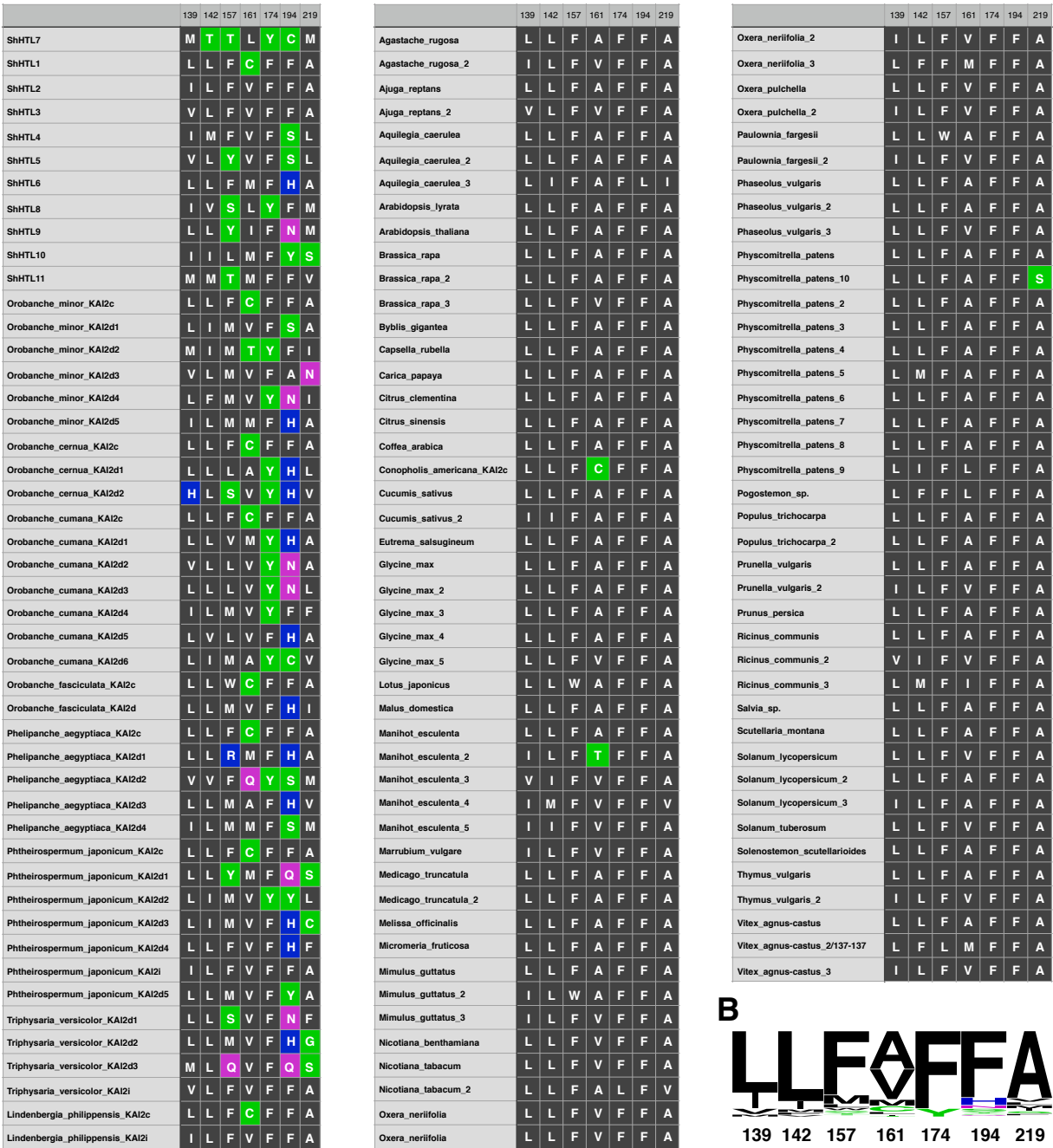


Fig. S7. Computational investigation on protein-ligand interactions of SPL7 in ShHTL7. (A) The process of the enzymatic reaction mechanism of SL hydrolysis catalyzed through the amino acid triad Ser-His-Asp. H246 in ShHTL7 acts as base that facilitates the nucleophilic attack to the carbonyl carbon of the D-ring by serine. **(B)** Putative binding

modes of SPL7 in *S*- and *R*-configuration in ShHTL7 obtained via IFD simulations (i.e. amino acid residues were treated flexibly during docking). The docking scores and ranks are as follows; (S)-SPL7, -10.196 kcal/mol (rank #2), (R)-SPL7, -8.763 kcal/mol (rank #3).

Figure S8

A



B



C

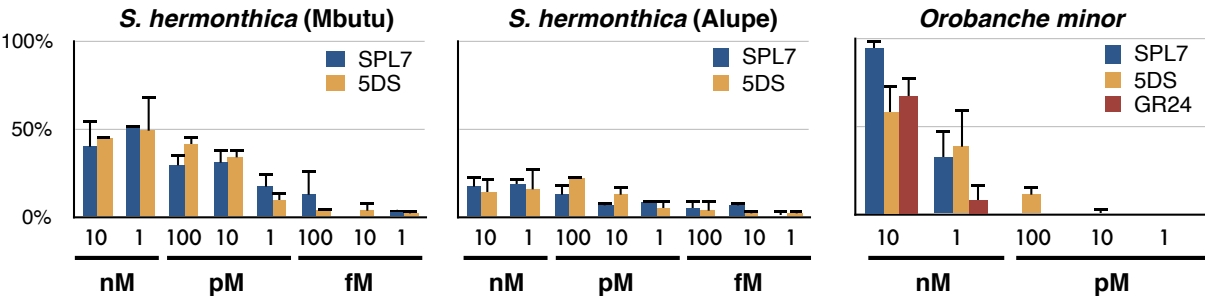


Fig. S8. Alignment of 7 essential active site residues responsible for ShHTL7 selectivity among HTL/KAI2 homologs. (A) HTL/KAI2 homologs in parasitic or non-parasitic plants from Orobanchaceae (left) or from other family (center and right) were shown. Sequence data was obtained

from (9). (B) Frequency plot of the seven amino acids created in WEBLOGO. (C) Germination of *S. hermonthica* ecotypes and *Orobancha minor* in response to SPL7. Mbutu, a harvest from mixed stands of sorghum, finger millet and maize filed in in Tanzania. Alupe, a harvest from maize filed in in Kenya.

Figure S9

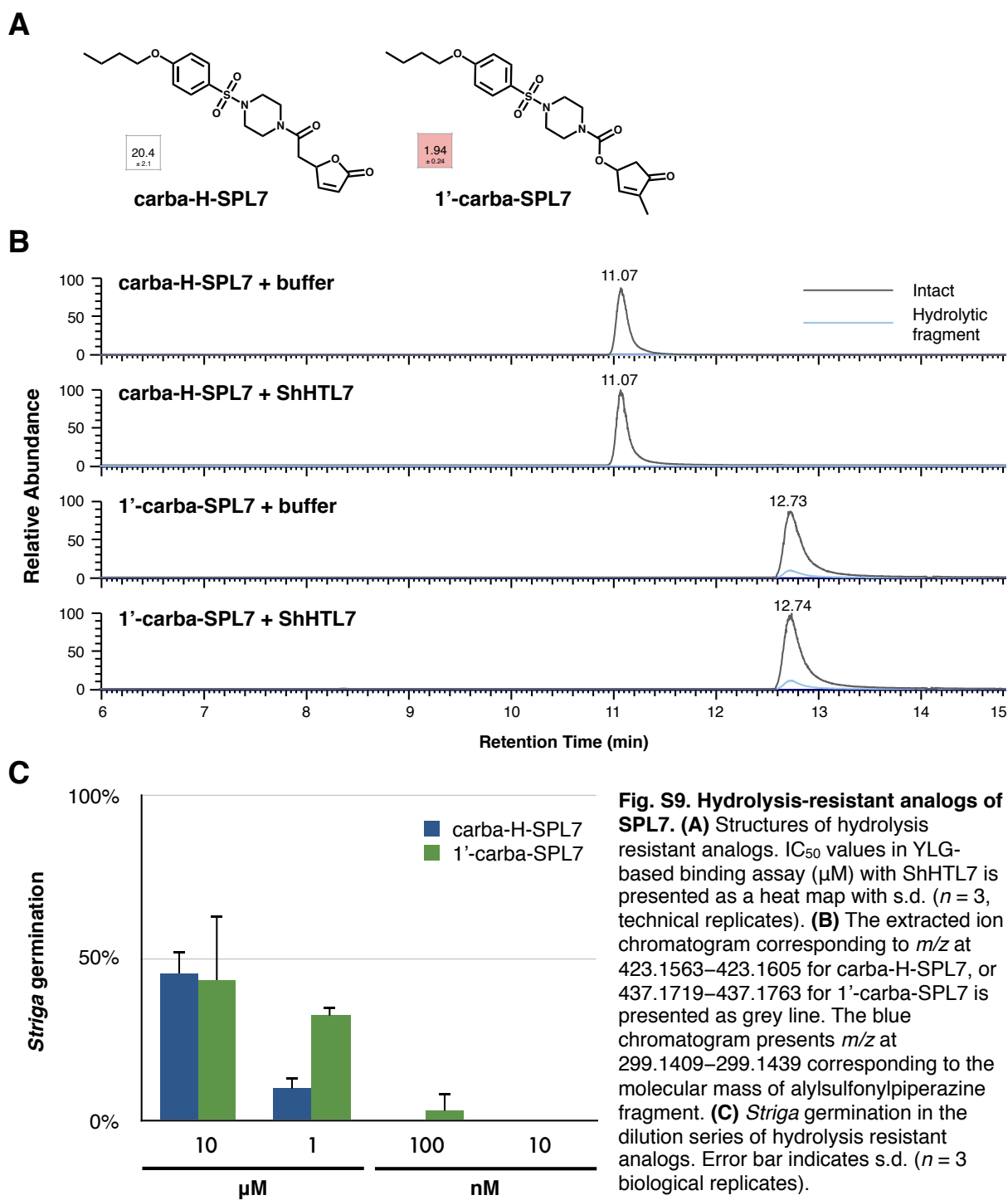


Figure S10

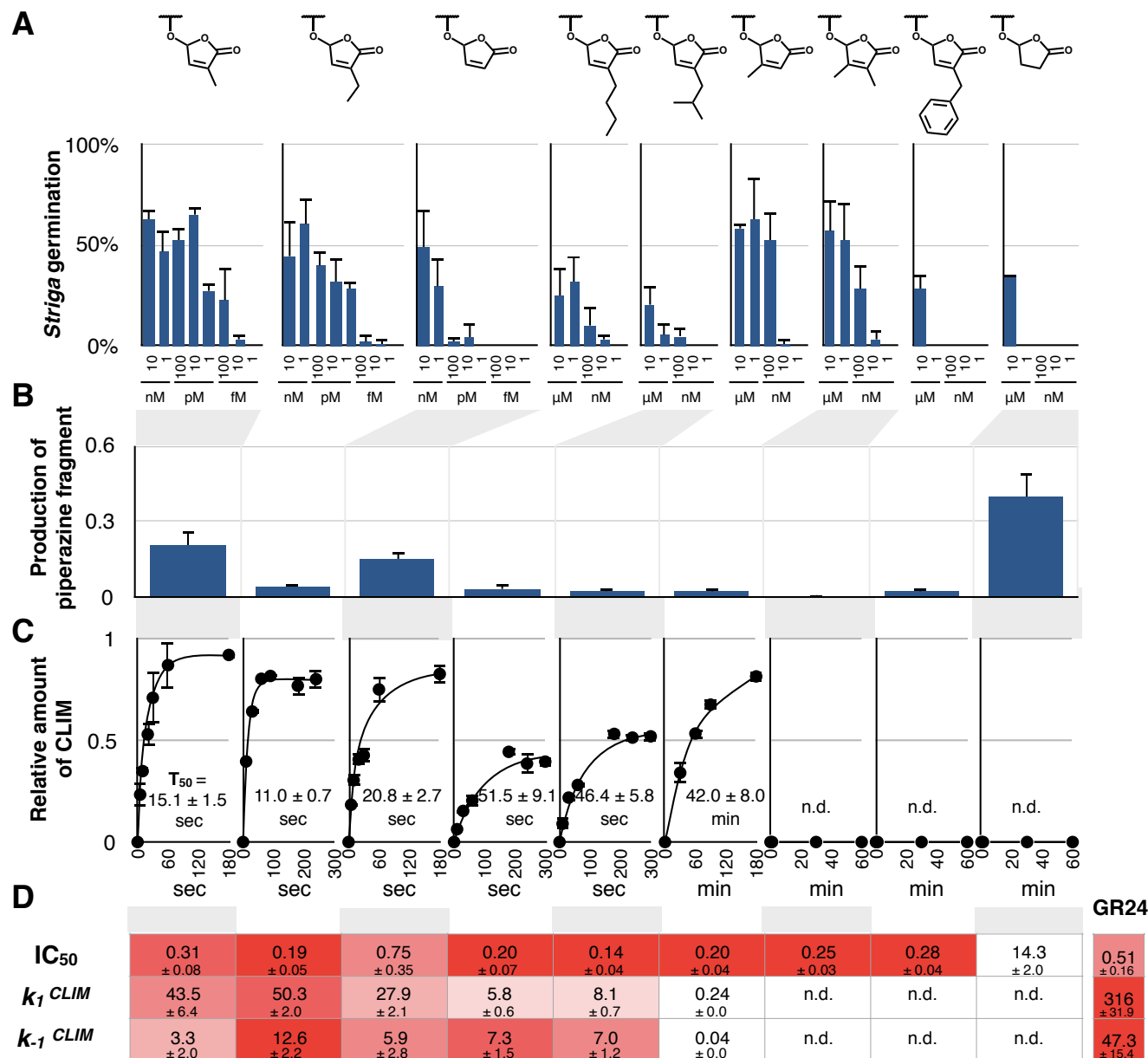


Fig. S10. SAR study with D-ring modified analogs of SPL7. (A) Germination of *Striga*. Error bar indicates s.d. ($n = 3$ biological replicates). While the MEC of the non-substituted version, H-SPL7, was at the pM level, the presence of a small linear alkyl group ($<C_4$) at the C4' position enhanced its MEC to the fM level. Increase in steric bulkiness of the C4'-substituent or methylation at the C3' position diminished its MEC to the nM level. Introducing benzyl group to the C4' position (Bn-SPL7) or saturating the double bond between C3' and C4' (sat-H-SPL7) caused a marked drop in germination activity (MEC = μ M level). **(B)** Production of the *N*-sulfonylpiperazine fragments. The quantity of liberated the piperazine fragments upon treatment of the analogs with ShHTL7 for 30 min was quantified by LC-MS. Relative values to complete digestion with KOH were shown. Error bar indicates s.d. ($n = 3$ technical replicates). Clear correlation of piperazine formation with MEC, except for sat-H-SPL7, indicated that the observed difference in potency is associated with the efficiency of the D-ring transfer. For sat-H-SPL7, while the

highest production of the piperazine fragment was observed, the CLIM formation process could not be traced by HPLC analysis under similar conditions, implying that the very short lifetime of sat-H-SPL7-derived CLIM led to low potency. **(C)** Time dependence of CLIM formation quantified by LC-MS. Error bar indicates s.d. ($n = 3$ technical replicates). Half-maximal time (T_{50}) was determined as time-of-arrival to 50% conversion of the steady state level. This analysis allowed directly assessing the correlation between potency and the D-ring transfer efficiency. Although CLIM formation was not detected in 3',4'-dimethyl, 4'-benzyl, or saturated analogs, T_{50} values of other analogs were proportional to their MEC. **(D)** Biochemical parameters for interaction with ShHTL7. IC₅₀ values (μ M) in the YLG assay with s.d. ($n = 3$, technical replicates) and reaction rate constants k_1^{CLIM} ($10^{-3}/\mu$ M/s) and k_{-1}^{CLIM} ($10^{-3}/s$) are presented as a heat map. n.d. = not detected. All IC₅₀ values are comparable except for sat-H-SPL7. Similar to T_{50} , k_1^{CLIM} values near linearly correlate with MEC while k_{-1}^{CLIM} seems to be unconnected to MEC.

Figure S11

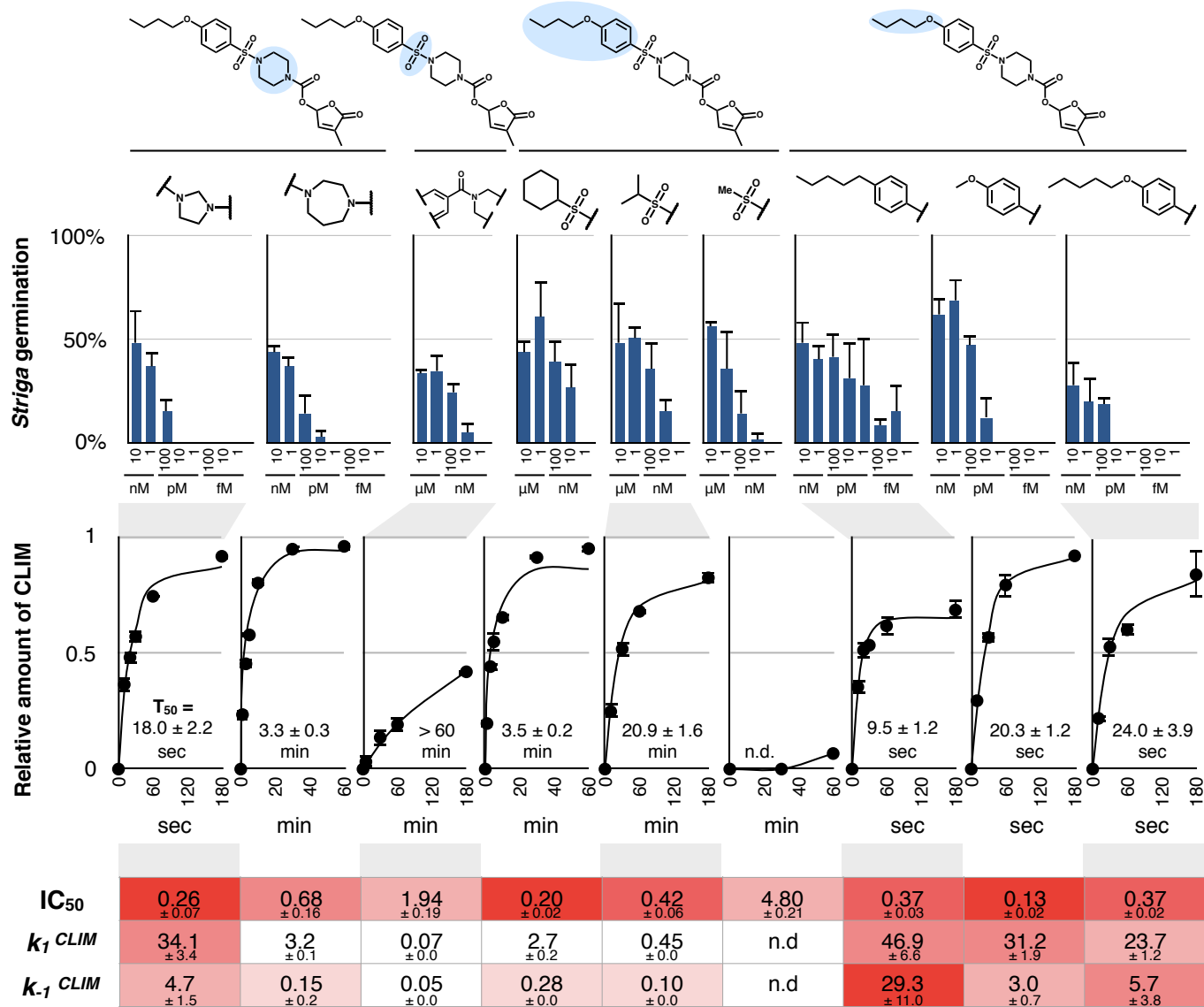


Fig. S11. SAR study with piperazine scaffold (the ABC-ring analog subunit) modified analogs of SPL7. The bar graph in the top panel represents germination of *Striga*. Error bar indicates s.d. ($n = 3$ biological replicates). The middle panel displays time-dependence of CLIM formation on ShHTL7, which was quantified by LC-MS. Error bar indicates s.d. ($n = 3$ technical replicates). Half-maximal time (T_{50}) was determined as time-of-arrival to 50% conversion of the steady state level. The bottom panel presents IC_{50} values (μM) with ShHTL7 in the YLG assay with s.d. ($n = 3$, technical replicates) and reaction rate constants k_1^{CLIM} ($10^{-3}/\mu M/s$) and k_{-1}^{CLIM} ($10^{-3}/s$) as a heat map. n.d. = not detected. In the case of modification of *N*-arylsulfonylpiperazine scaffold of SPL7s without altering the D-ring structure, not only k_{-1}^{CLIM} but also the other parameters, MEC, IC_{50} , T_{50} , and k_1^{CLIM} values, were not correlated. Regarding the piperazine unit of SPL7, the MEC was not sensitive to the ring size, as 5- and 7-membered ring derivatives resulted in equal losses in MEC to the pM level without affecting IC_{50} . However, this ring-size modification made a large difference in the T_{50} or k_1^{CLIM} values. The importance of the hydrogen-

bond-accepting SO_2 group was confirmed by changing it to a carbonyl moiety, leading to marked decreases in MEC and IC_{50} with significant reduction of the rate of CLIM formation. Structural modifications of the *p*-butoxyphenyl group on the SO_2 moiety caused uncorrelated changes in the parameters. For instance, replacement of the aromatic nuclei with an aliphatic alkyl group generally reduced MEC to the nM range, although the IC_{50} , T_{50} , and k_1^{CLIM} values gradually decreased as the steric demand of the sulfonyl substituent was reduced. Finally, CLIM formation from *N*-methylsulfonyl derivative (Ms-SPL7) could not be traced by LC-MS within the experimental timescale. Furthermore, even slight alteration to the length of the *para*-alkoxy group in the arylsulfonyl unit decreased MEC by three orders of magnitude with concomitant retardation of the CLIM formation rate, while IC_{50} values were not significantly affected. In contrast, replacing the oxygen atom in the *para*-butoxy appendage with a methylene group kept all parameters constant.

Figure S12

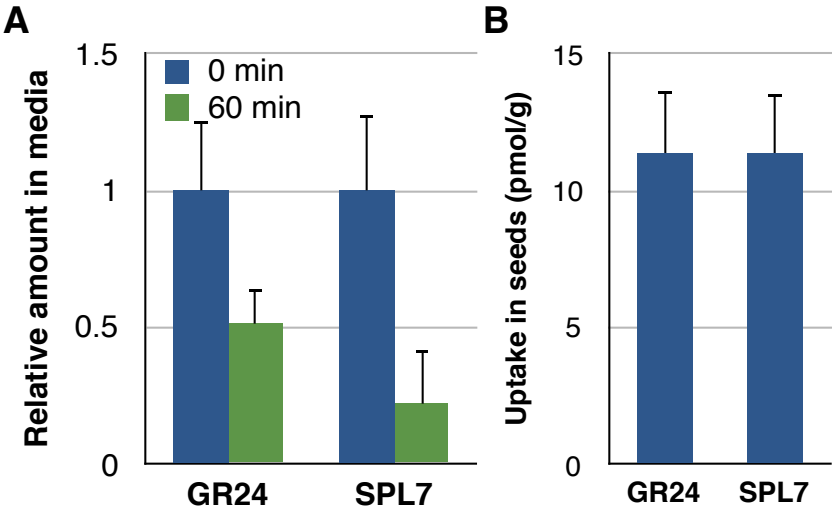


Fig. S12. Uptake of (+)-GR24 and SPL7 by *Striga* seeds. (A) Reduction of SL agonists in the media due to uptake by *Striga* seeds. 10 nM of (+)-GR24 and SPL7 were applied together to *Striga* seeds for 60 min. Relative amounts to t = 0 were presented with s.d. (n = 3 biological replicates). (B) The amount of (+)-GR24 and SPL7 up-taken by *Striga* seeds. The agonists were extracted from the *Striga* seeds in (A) and monitored by LC-MS. (n = 3 biological replicates). Increases of degradation products (the ABC-ring or the piperazine fragment) during incubation were not observed.

Figure S13

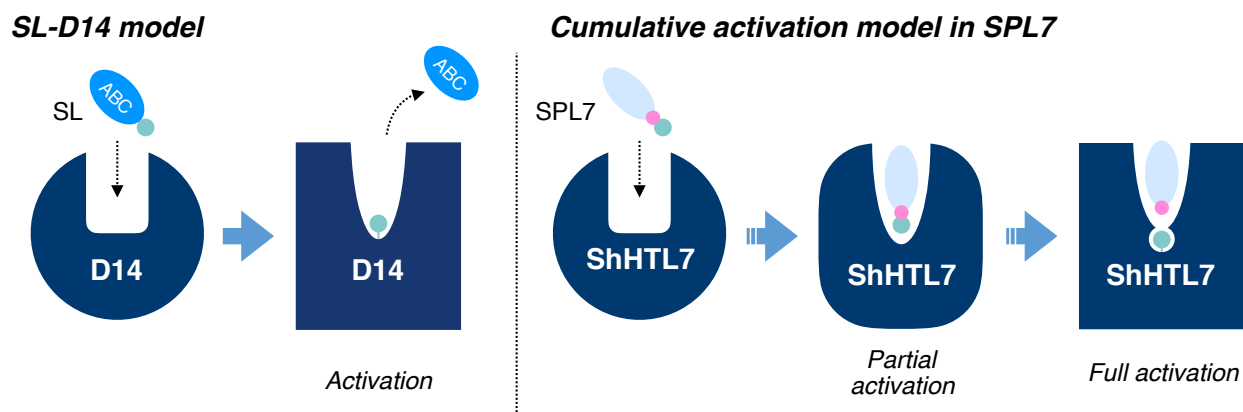
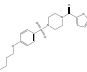
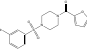
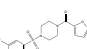
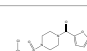
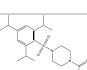
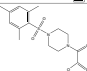
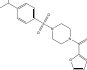
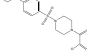
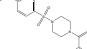
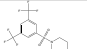
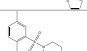
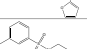
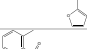
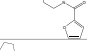
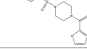
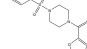
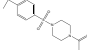
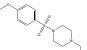
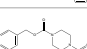
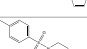
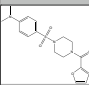
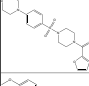
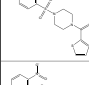
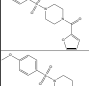
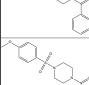
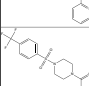
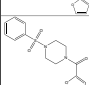
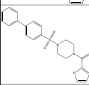
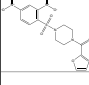
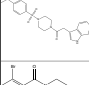
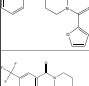
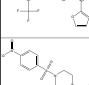
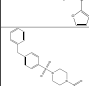
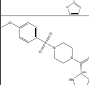
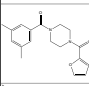
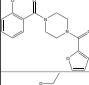
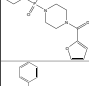
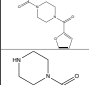
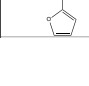




Fig. S13 Cumulative activation model of SPL7. (Left) Proposed model for activation of D14 SL receptor (7, 14). As a consequence of hydrolysis of SLs, the D-ring is covalently attached to catalytic histidine residue to form CLIM. On the other hand, ABC-ring is released from the pocket before activating downstream ubiquitin-dependent proteasomal

pathway. (Right) Cumulative activation model in SPL7 hypothesized in this study. In contrast to the SL-D14 model, ShHTL7 can be partially activated without CLIM formation. The ABC-portion of SPL7 has additional functions after CLIM formation to gain fM-range potency.

Table S1. Structure and numeric data for fig. S1B

ID	Structure	Striga germination	YLG assay with 10 μ M of competitive molecules									
			ShHTL2	ShHTL3	ShHTL4	ShHTL5	ShHTL6	ShHTL7	ShHTL8	ShHTL9	ShHTL10	ShHTL11
DMSO	-	0% \pm 0%	1	1	1	1	1	1	1	1	1	1
SAM-690		29.4% \pm 14.8%	1.00 \pm 0.06	0.95 \pm 0.06	0.82 \pm 0.08	0.93 \pm 0.03	0.94 \pm 0.05	0.29 \pm 0.07	1.00 \pm 0.03	1.06 \pm 0.05	1.02 \pm 0.13	1.02 \pm 0.01
S-mBr		28.9% \pm 4.0%	0.78 \pm 0.06	0.98 \pm 0.01	0.90 \pm 0.11	0.96 \pm 0.06	0.91 \pm 0.07	0.19 \pm 0.05	1.01 \pm 0.04	0.96 \pm 0.02	0.99 \pm 0.04	0.95 \pm 0.03
S-mF		34.1% \pm 6.2%	0.85 \pm 0.04	1.02 \pm 0.06	1.02 \pm 0.01	1.00 \pm 0.01	0.90 \pm 0.04	0.57 \pm 0.10	1.03 \pm 0.03	0.99 \pm 0.06	0.95 \pm 0.10	0.86 \pm 0.04
S-dlc		36.2% \pm 0.7%	0.69 \pm 0.07	0.86 \pm 0.02	0.85 \pm 0.03	0.97 \pm 0.02	0.87 \pm 0.02	0.25 \pm 0.06	0.79 \pm 0.02	0.97 \pm 0.07	1.05 \pm 0.03	0.91 \pm 0.02
SAM-12		0.0% \pm 0.0%	1.25 \pm 0.07	1.54 \pm 0.13	1.01 \pm 0.15	1.06 \pm 0.04	0.92 \pm 0.03	0.21 \pm 0.00	0.87 \pm 0.04	0.86 \pm 0.01	1.10 \pm 0.02	1.03 \pm 1.03
SAM-25		13.5% \pm 2.7%	1.17 \pm 0.07	1.40 \pm 0.02	0.96 \pm 0.11	0.99 \pm 0.02	1.08 \pm 0.02	0.28 \pm 0.07	0.88 \pm 0.02	0.86 \pm 0.02	1.03 \pm 0.03	0.91 \pm 0.54
SAM-31		11.1% \pm 0.0%	1.14 \pm 0.07	1.18 \pm 0.10	1.05 \pm 0.05	1.04 \pm 0.01	0.89 \pm 0.08	0.33 \pm 0.03	1.00 \pm 0.04	0.91 \pm 0.05	1.10 \pm 0.06	1.05 \pm 0.24
SAM-43		3.1% \pm 4.4%	1.12 \pm 0.10	1.31 \pm 0.09	0.89 \pm 0.04	0.99 \pm 0.01	0.86 \pm 0.15	0.33 \pm 0.08	0.97 \pm 0.15	1.00 \pm 0.02	1.03 \pm 0.03	0.98 \pm 0.58
SAM-30		36.5% \pm 21.3%	1.08 \pm 0.17	1.30 \pm 0.03	0.90 \pm 0.06	1.03 \pm 0.01	0.91 \pm 0.11	0.37 \pm 0.10	1.00 \pm 0.05	0.95 \pm 0.04	1.07 \pm 0.04	1.03 \pm 0.47
SAM-15		13.5% \pm 13.6%	1.29 \pm 0.08	1.46 \pm 0.07	1.03 \pm 0.11	1.01 \pm 0.01	1.07 \pm 0.12	0.38 \pm 0.01	1.02 \pm 0.08	0.95 \pm 0.01	1.10 \pm 0.07	1.05 \pm 0.30
SAM-32		2.9% \pm 4.2%	1.16 \pm 0.05	1.27 \pm 0.07	1.03 \pm 0.17	1.03 \pm 0.06	1.01 \pm 0.11	0.38 \pm 0.00	0.99 \pm 0.07	0.95 \pm 0.03	1.09 \pm 0.06	0.93 \pm 1.22
SAM-17		40.8% \pm 5.6%	1.14 \pm 0.25	1.54 \pm 0.03	1.10 \pm 0.16	1.10 \pm 0.03	1.02 \pm 0.00	0.55 \pm 0.01	0.99 \pm 0.01	1.00 \pm 0.00	1.04 \pm 0.07	0.97 \pm 0.93
SAM-16		44.4% \pm 15.7%	1.05 \pm 0.04	1.09 \pm 0.04	1.04 \pm 0.04	1.03 \pm 0.03	0.95 \pm 0.09	0.61 \pm 0.05	0.96 \pm 0.01	0.95 \pm 0.04	1.07 \pm 0.03	0.94 \pm 0.80
SAM-44		24.4% \pm 3.1%	1.07 \pm 0.02	1.30 \pm 0.08	1.04 \pm 0.08	0.99 \pm 0.03	1.00 \pm 0.14	0.62 \pm 0.01	1.05 \pm 0.13	1.02 \pm 0.01	1.07 \pm 0.03	1.05 \pm 0.51
SAM-6		0.0% \pm 0.0%	1.00 \pm 0.03	1.16 \pm 0.11	0.91 \pm 0.08	1.01 \pm 0.05	0.96 \pm 0.02	0.65 \pm 0.06	1.00 \pm 0.03	0.99 \pm 0.02	0.97 \pm 0.04	1.01 \pm 0.61
SAM-26		18.9% \pm 5.5%	1.21 \pm 0.06	1.41 \pm 0.09	0.94 \pm 0.19	1.05 \pm 0.01	0.97 \pm 0.05	0.68 \pm 0.02	1.04 \pm 0.07	1.04 \pm 0.03	1.08 \pm 0.02	1.11 \pm 0.02
SAM-35		9.6% \pm 4.7%	1.18 \pm 0.10	1.44 \pm 0.04	0.94 \pm 0.16	1.01 \pm 0.02	1.01 \pm 0.07	0.69 \pm 0.02	1.03 \pm 0.15	0.97 \pm 0.05	1.12 \pm 0.01	1.02 \pm 0.46
SAM-41		0.0% \pm 0.0%	1.36 \pm 0.04	1.59 \pm 0.04	1.14 \pm 0.10	1.06 \pm 0.03	1.03 \pm 0.02	0.70 \pm 0.07	0.98 \pm 0.02	0.93 \pm 0.11	1.00 \pm 0.04	0.96 \pm 0.71
SAM-7		1.7% \pm 2.4%	1.07 \pm 0.05	1.16 \pm 0.03	1.00 \pm 0.03	1.02 \pm 0.03	1.00 \pm 0.09	0.72 \pm 0.02	1.02 \pm 0.00	1.01 \pm 0.06	1.01 \pm 0.02	1.06 \pm 0.99
SAM-34		0.0% \pm 0.0%	1.16 \pm 0.07	1.41 \pm 0.10	0.90 \pm 0.07	1.05 \pm 0.03	0.98 \pm 0.08	0.72 \pm 0.05	1.01 \pm 0.20	0.93 \pm 0.09	1.08 \pm 0.04	1.10 \pm 0.45

ID	Structure	Striga germination	YLG assay with 10 μ M of competitive molecules									
			ShHTL2	ShHTL3	ShHTL4	ShHTL5	ShHTL6	ShHTL7	ShHTL8	ShHTL9	ShHTL10	ShHTL11
SAM-46		12.9% \pm 1.9%	1.09 \pm 0.17	1.11 \pm 0.07	1.20 \pm 0.17	0.99 \pm 0.08	1.01 \pm 0.15	0.75 \pm 0.11	1.01 \pm 0.13	1.06 \pm 0.01	1.06 \pm 0.03	1.12 \pm 0.23
SAM-45		7.7% \pm 10.9%	1.12 \pm 0.03	1.16 \pm 0.03	1.05 \pm 0.08	0.99 \pm 0.02	1.03 \pm 0.18	0.78 \pm 0.06	1.04 \pm 0.14	1.05 \pm 0.07	1.08 \pm 0.03	1.07 \pm 0.07
SAM-40		2.4% \pm 3.4%	1.09 \pm 0.03	1.26 \pm 0.03	0.98 \pm 0.10	1.05 \pm 0.01	0.93 \pm 0.10	0.79 \pm 0.09	0.99 \pm 0.04	1.03 \pm 0.05	1.12 \pm 0.01	1.05 \pm 0.95
SAM-27		0.0% \pm 0.0%	1.17 \pm 0.04	1.36 \pm 0.06	0.94 \pm 0.16	1.00 \pm 0.01	1.04 \pm 0.18	0.82 \pm 0.05	1.03 \pm 0.17	1.02 \pm 0.01	1.12 \pm 0.02	1.01 \pm 0.35
SAM-39		0.0% \pm 0.0%	1.14 \pm 0.05	1.12 \pm 0.02	0.99 \pm 0.11	1.04 \pm 0.01	0.98 \pm 0.20	0.82 \pm 0.03	1.05 \pm 0.16	1.08 \pm 0.01	1.12 \pm 0.02	1.17 \pm 0.41
SAM-37		0.0% \pm 0.0%	1.09 \pm 0.10	1.17 \pm 0.10	0.90 \pm 0.16	1.05 \pm 0.02	1.03 \pm 0.16	0.86 \pm 0.02	1.02 \pm 0.15	1.01 \pm 0.02	1.09 \pm 0.02	1.13 \pm 0.40
SAM-9		0.0% \pm 0.0%	1.23 \pm 0.12	1.52 \pm 0.03	1.02 \pm 0.11	1.05 \pm 0.03	1.00 \pm 0.03	0.88 \pm 0.08	1.00 \pm 0.02	1.02 \pm 0.02	1.06 \pm 0.05	1.02 \pm 0.80
SAM-10		0.0% \pm 0.0%	1.22 \pm 0.02	1.41 \pm 0.01	1.06 \pm 0.14	1.06 \pm 0.02	1.00 \pm 0.02	0.89 \pm 0.01	1.02 \pm 0.06	1.03 \pm 0.01	1.02 \pm 0.04	1.04 \pm 0.44
SAM-28		9.3% \pm 2.6%	1.18 \pm 0.02	1.31 \pm 0.09	1.00 \pm 0.19	1.07 \pm 0.01	1.03 \pm 0.12	0.93 \pm 0.02	1.03 \pm 0.11	1.00 \pm 0.03	1.13 \pm 0.03	1.07 \pm 0.57
SAM-33		0.0% \pm 0.0%	1.28 \pm 0.07	1.53 \pm 0.03	1.04 \pm 0.02	0.98 \pm 0.01	1.02 \pm 0.00	0.95 \pm 0.08	1.04 \pm 0.07	0.86 \pm 0.13	1.02 \pm 0.02	1.00 \pm 0.51
SAM-38		3.8% \pm 5.4%	1.12 \pm 0.05	1.27 \pm 0.08	0.99 \pm 0.12	1.04 \pm 0.02	1.10 \pm 0.12	0.95 \pm 0.04	1.02 \pm 0.10	1.03 \pm 0.00	1.07 \pm 0.06	1.07 \pm 0.14
SAM-2		0.0% \pm 0.0%	1.13 \pm 0.15	1.28 \pm 0.05	1.07 \pm 0.05	1.02 \pm 0.01	1.01 \pm 0.00	0.96 \pm 0.03	1.00 \pm 0.16	0.99 \pm 0.03	1.01 \pm 0.04	0.98 \pm 0.73
SAM-5		7.1% \pm 10.1%	1.11 \pm 0.02	1.22 \pm 0.02	0.95 \pm 0.14	1.00 \pm 0.06	1.02 \pm 0.04	0.97 \pm 0.02	0.99 \pm 0.04	1.03 \pm 0.03	1.01 \pm 0.07	0.98 \pm 0.43
SAM-11		0.0% \pm 0.0%	1.10 \pm 0.07	1.25 \pm 0.10	0.98 \pm 0.09	1.05 \pm 0.02	1.01 \pm 0.13	0.98 \pm 0.04	1.01 \pm 0.13	1.03 \pm 0.02	1.04 \pm 0.02	0.99 \pm 0.43
SAM-29		0.0% \pm 0.0%	1.09 \pm 0.09	1.27 \pm 0.14	0.95 \pm 0.20	1.04 \pm 0.02	1.03 \pm 0.14	0.99 \pm 0.00	1.03 \pm 0.06	1.02 \pm 0.04	1.07 \pm 0.05	1.08 \pm 0.98
SAM-36		0.0% \pm 0.0%	1.17 \pm 0.06	1.28 \pm 0.07	1.07 \pm 0.09	1.02 \pm 0.06	1.06 \pm 0.09	1.00 \pm 0.01	1.07 \pm 0.17	1.06 \pm 0.02	1.15 \pm 0.03	1.19 \pm 0.21
SAM-3		0.0% \pm 0.0%	1.11 \pm 0.06	1.26 \pm 0.02	1.00 \pm 0.10	0.99 \pm 0.04	1.03 \pm 0.02	1.02 \pm 0.07	1.02 \pm 0.04	1.00 \pm 0.04	1.06 \pm 0.06	1.00 \pm 0.46
SAM-4		0.0% \pm 0.0%	1.12 \pm 0.05	1.25 \pm 0.02	1.02 \pm 0.09	1.05 \pm 0.05	1.03 \pm 0.06	1.02 \pm 0.10	1.02 \pm 0.12	1.02 \pm 0.00	1.03 \pm 0.06	1.03 \pm 0.51
SAM-21		0.0% \pm 0.0%	1.09 \pm 0.05	1.36 \pm 0.05	1.09 \pm 0.05	1.03 \pm 0.03	1.04 \pm 0.11	1.02 \pm 0.01	1.03 \pm 0.06	1.05 \pm 0.06	1.06 \pm 0.06	1.04 \pm 0.57
SAM-1		0.0% \pm 0.0%	1.11 \pm 0.07	1.40 \pm 0.09	1.06 \pm 0.05	1.05 \pm 0.02	1.03 \pm 0.05	1.03 \pm 0.01	1.02 \pm 0.03	0.97 \pm 0.06	1.02 \pm 0.03	1.04 \pm 0.16
SAM-13		0.0% \pm 0.0%	1.17 \pm 0.10	1.29 \pm 0.21	1.00 \pm 0.09	1.03 \pm 0.03	1.03 \pm 0.13	1.05 \pm 0.01	1.02 \pm 0.09	1.03 \pm 0.02	1.08 \pm 0.05	1.10 \pm 0.61

ID	Structure	Striga germination	YLG assay with 10 µM of competitive molecules									
			ShHTL2	ShHTL3	ShHTL4	ShHTL5	ShHTL6	ShHTL7	ShHTL8	ShHTL9	ShHTL10	ShHTL11
SAM-18		0.0% ± 0.0%	1.15 ± 0.10	1.36 ± 0.08	0.96 ± 0.19	1.04 ± 0.01	1.02 ± 0.01	1.06 ± 0.02	1.02 ± 0.08	1.02 ± 0.01	1.03 ± 0.02	1.11 ± 0.36
SAM-19		0.0% ± 0.0%	1.17 ± 0.07	1.40 ± 0.06	0.98 ± 0.15	1.08 ± 0.01	1.04 ± 0.08	1.06 ± 0.02	1.04 ± 0.10	1.04 ± 0.04	1.09 ± 0.01	1.15 ± 0.27
SAM-22		0.0% ± 0.0%	1.12 ± 0.07	1.34 ± 0.07	1.11 ± 0.00	1.02 ± 0.04	0.99 ± 0.10	1.06 ± 0.08	1.00 ± 0.06	1.07 ± 0.03	1.05 ± 0.04	1.02 ± 0.28
SAM-23		0.0% ± 0.0%	1.10 ± 0.04	1.14 ± 0.09	1.08 ± 0.05	1.03 ± 0.01	1.03 ± 0.11	1.06 ± 0.00	1.04 ± 0.11	1.07 ± 0.08	1.07 ± 0.04	1.14 ± 1.25
SAM-24		0.0% ± 0.0%	1.14 ± 0.08	1.24 ± 0.15	0.97 ± 0.12	1.01 ± 0.03	1.00 ± 0.09	1.06 ± 0.01	1.00 ± 0.18	1.05 ± 0.08	1.13 ± 0.01	1.08 ± 1.35
SAM-20		0.0% ± 0.0%	1.16 ± 0.11	1.36 ± 0.03	1.08 ± 0.13	1.07 ± 0.02	1.02 ± 0.07	1.07 ± 0.00	1.05 ± 0.17	1.07 ± 0.05	1.13 ± 0.01	1.09 ± 0.74
SAM-14		0.0% ± 0.0%	1.20 ± 0.03	1.29 ± 0.02	1.06 ± 0.11	1.00 ± 0.04	1.04 ± 0.07	1.10 ± 0.03	1.00 ± 0.05	1.09 ± 0.03	1.06 ± 0.04	1.10 ± 0.13
M-diox		41.7% ± 9.2%	1.07 ± 0.05	0.81 ± 0.03	0.98 ± 0.04	0.93 ± 0.02	0.84 ± 0.01	0.67 ± 0.06	0.91 ± 0.06	0.92 ± 0.05	0.88 ± 0.10	0.95 ± 0.04
M-odiF		14.1% ± 3.6%	1.04 ± 0.13	0.62 ± 0.02	0.63 ± 0.02	0.77 ± 0.07	0.90 ± 0.04	0.60 ± 0.06	0.97 ± 0.04	0.94 ± 0.00	1.00 ± 0.00	0.85 ± 0.07
SAM-M10		70.7% ± 3.8%	1.05 ± 0.02	1.11 ± 0.04	0.75 ± 0.00	1.05 ± 0.02	0.89 ± 0.22	0.66 ± 0.11	0.94 ± 0.14	0.66 ± 0.06	1.16 ± 0.00	0.92 ± 0.25
SAM-M4		2.9% ± 4.2%	1.24 ± 0.08	1.36 ± 0.02	1.08 ± 0.13	1.13 ± 0.03	0.90 ± 0.14	0.73 ± 0.03	0.93 ± 0.12	0.93 ± 0.12	1.09 ± 0.04	0.99 ± 1.02
SAM-M8		4.2% ± 5.9%	1.03 ± 0.04	1.09 ± 0.04	1.02 ± 0.04	1.04 ± 0.04	1.02 ± 0.15	0.80 ± 0.07	0.98 ± 0.11	0.95 ± 0.00	1.10 ± 0.02	0.94 ± 0.21
SAM-M2		0.0% ± 0.0%	1.14 ± 0.02	1.18 ± 0.08	1.06 ± 0.08	1.02 ± 0.02	1.01 ± 0.13	0.81 ± 0.10	1.01 ± 0.09	1.04 ± 0.08	1.14 ± 0.08	0.97 ± 1.15
SAM-M1		0.0% ± 0.0%	1.02 ± 0.13	0.95 ± 0.13	1.03 ± 0.07	1.02 ± 0.01	1.00 ± 0.17	0.88 ± 0.01	1.01 ± 0.03	1.04 ± 0.01	1.09 ± 0.04	1.04 ± 0.04
SAM-M5		0.0% ± 0.0%	1.12 ± 0.05	1.30 ± 0.02	0.93 ± 0.17	1.06 ± 0.03	1.04 ± 0.19	0.95 ± 0.04	1.00 ± 0.12	0.92 ± 0.12	1.09 ± 0.02	0.96 ± 0.06
SAM-M3		0.0% ± 0.0%	1.35 ± 0.07	1.72 ± 0.07	0.99 ± 0.20	1.10 ± 0.03	1.06 ± 0.09	0.98 ± 0.09	1.03 ± 0.01	1.02 ± 0.14	1.02 ± 0.03	1.02 ± 0.80
SAM-M6		4.5% ± 6.4%	1.11 ± 0.04	1.31 ± 0.06	1.05 ± 0.11	1.04 ± 0.08	1.05 ± 0.24	0.98 ± 0.01	1.03 ± 0.18	1.02 ± 0.05	1.07 ± 0.07	1.06 ± 0.42
SAM-M9		0.0% ± 0.0%	1.05 ± 0.03	1.15 ± 0.07	1.09 ± 0.06	1.07 ± 0.02	1.02 ± 0.17	0.99 ± 0.04	1.02 ± 0.15	1.06 ± 0.07	1.11 ± 0.02	1.05 ± 0.57
SAM-M7		2.8% ± 3.9%	1.11 ± 0.04	1.25 ± 0.02	1.01 ± 0.13	1.03 ± 0.05	1.03 ± 0.22	1.01 ± 0.03	1.05 ± 0.18	1.03 ± 0.02	1.07 ± 0.06	1.06 ± 0.98
GR24	-	61.4% ± 5.1%	0.87 ± 0.07	1.06 ± 0.15	0.15 ± 0.11	0.59 ± 0.03	0.06 ± 0.04	0.12 ± 0.16	0.20 ± 0.13	0.16 ± 0.06	0.04 ± 0.03	0.16 ± 0.08